Bachelor's Thesis

Untersuchung des antimikrobiellen Effekts von Dermcidin mithilfe von Computersimulationen

Investigation of dermcidins antimicrobial effect with computer simulation

prepared by

Bartosz F. Guzek

from Katowice

at the Max Planck lnstitute for Biophysical Chemistry

Thesis period:	1st July 2014 until 6th October 2014
First referee:	Prof. Dr. Bert L. de Groot
Second referee:	Prof. Dr. Karl Helmut Grubmüller

Abstract

Due to growing multiresistance of bacteria new sources for antibiotics are needed. A promising way out of this problem could be antimicrobial peptides (AMP) which are currently investigated by pharmaceutical companies. An example for such an AMP is dermcidin which can be found on the human skin. It shows antimicrobial activity by presumably forming ion channels in bacterial membranes.
In this study we use molecular dynamics simulations to investigate the effect of mutations on the conductance of dermcidin. For this purpose the residues that mostly influence the channel radius are mutated. The resulting conductance primarily depends on the position of the residue that was mutated and only secondarily on the radius of the channel. Furthermore, an opening/closing behaviour, which includes the motion of the backbones and several residues, is observed. By using simulations we demonstrate that the conductance also depends on whether the channel is in an open or a closed state. At the end we show that mutations - raising the conductance and also positively affecting other properties which are crucial for antimicrobial activity - are possible.

Zusammenfassung

Aufgrund der entstehenden Multiresistenz von Bakterien werden neue Quellen für Antibiotika benötigt. Einen vielversprechenden Ausweg aus diesem Problem könnten die antimikrobiellen Peptide (AMP) darstellen, die derzeit von Pharmaunternehmen untersucht werden. Ein Beispiel für ein solchen AMP ist Dermcidin, das sich auf der menschlichen Haut befindet. Es wirkt vermutlich durch Bildung von Ionenkanäle in Bakterienmembranen antimikrobiell.
In dieser Studie verwenden wir Molekulardynamik-Simulationen, um die Wirkung von Mutationen auf die Leitfähigkeit von Dermcidin zu untersuchen. Zu diesem Zweck werden Mutationen von Aminosäureresten, die am meisten den Ionenkanalradius beeinflussen, durchgeführt. Die resultierenden Leitfähigkeiten hängen primär von der Position des Aminosäurerests, der mutiert wurde, und sekundär von dem daraus entstehendem Radiusprofil des Kanals, ab. Ferner wird ein Öffnungs-/Schließungmechanismus, der die Bewegung der Hauptketten und mehrerer Aminosäurereste umfasst, beobachtet. Durch Simulationen zeigen wir, dass die Leitfähigkeit auch davon abhängt, inwieweit sich der Ionenkanal in einem geschlossen oder geöffneten Zustand befindet. Am Ende zeigen wir, dass Mutationen durchgeführt werden können, die gleichzeitig die Leitfähigkeit erhöhen und sich positiv auf andere Eigenschaften, die entscheidend für die antimikrobielle Aktivität von Dermcidin sind, auswirken.

Contents

Nomenclature

Abbreviations	Meaning
aAMP	Anionic AntiMicrobial Peptide
AMP	AntiMicrobial Peptide
cAMP	Cationic AntiMicrobial Peptide
C36	CHARMM36 force field
CEP	Computational ElectroPhoresis
ED	Essential Dynamics
EV	EigenVector
FF	Force Field
CHARMM	Chemistry at HARvard Molecular Mechanics
GROMACS	GROningen MAchine for Chemical Simulations
PCA	Principal Component Analysis
POPE	1-Palmitoyl-2-Oleoyl-PhosphatidylEthanolamine
POPG	1-Palmitoyl-2-Oleoyl-PhosphatidylGlycerol
PLS FMA	Partial Least Square Functional Mode Analysis
MD	Molecular Dynamics
TMV	TransMembrane Voltage
WT	Wild Type

1. Introduction

One can say that one of the greatest medical developments of the 20th century are antibiotics. The majority of the classes of antibiotic agents were discovered in the „golden era“of antibiotics, namely in the 40s to 60s.
Antibiotics are referred to as antibacterial drugs, which inhibit the growth or survival of bacteria without damaging the eukaryotic host. To achieve this objective, antibiotics interfere the cell wall synthesis, the protein synthesis or DNA replication of the bacteria. In each of these three possibilities, antibiotics use biochemical differences between prokaryotic and eukaryotic cells in order to act selectively [63].
Meanwhile, more and more bacteria are developing resistance to the antibiotics available on the market, so that the exploration of novel drugs is increasingly important [46]. A possible way out of this difficult situation may offer antimicrobial peptides (AMP). These are part of the natural defence mechanism of most living beings and show antimicrobial activity against a broad spectrum of bacteria, fungi and enveloped viruses [52]. Using phylogenetic analysis of the AMP β-defensin, it was possible to trace its gene to a over a half billion year old gene [53]. Despite their ancient origin, they show a high activity against multiresistance bacteria, so that they become an subject of the research in novel antibiotics.
As it can be difficult to achieve the required concentration of an active ingredient at the target organism, an increased antimicrobial effect could be needed to even out the low concentration.
This bachelor thesis concerns about the AMP dermcidin, which can be found on human skin, is part of the human immune system and kills bacteria by forming ion channels on the bacteria membranes [52]. Thus the idea behind this bachelor thesis is, that it should be possible to increase dermcidins antimicrobial properties by increasing the conductance of the ion channel, that is formed by six dermcidin monomers, through mutations. As the antimicrobial effect of dermcidin also depends on other properties than its conductance, they should also be increased or at least conserved.

2. Basic principles of relevant biological systems

2.1. Cell membrane

To understand the mode of action of AMPs and antibiotics that act on the cell membrane, a basic knowledge about the bacterial cell membrane and its differences to the eukaryotic membrane is needed. Not only the question how antibiotics act on the bacterial membrane, but also why they do not attack eukaryotic membranes will be discussed in the following text.
The cell membrane is an essential part of the cell structure for all organisms: it defines the shape of the cell and maintains fundamental differences, like the ion concentration between the cytosol and the extracellular surrounding. Only with this spatial separation and the high impermeability of the membrane to water soluble molecules the cell can use the ion gradient across the membrane, for example, for synthesis of adenosine triphosphate (ATP).
The structure of all biological membranes features the same basic construction: continuous bilayer with a thickness of about $4-10\,\mathrm{nm}$ (see fig. 2.1 C). It consists mostly of lipids and protein molecules which are held together by non-covalent interactions. Due to the fluid nature of the membrane its components are able to move in the plane on the membrane [3, p. 583ff.]. The most widespread lipid in membranes is phospholipid, so that the following text will concentrate only on this lipid.

2.1.1. Membrane lipids

Lipid molecules in the membrane are called amphipathic. They have a hydrophilic/ polar head group consisting of phosphate, glycerol or sphingosine, an organic group like choline and two hydrophobic/non-polar tails from which usually one has one or more cis-double bonds (see fig. 2.1 B). Based on the described shape and the

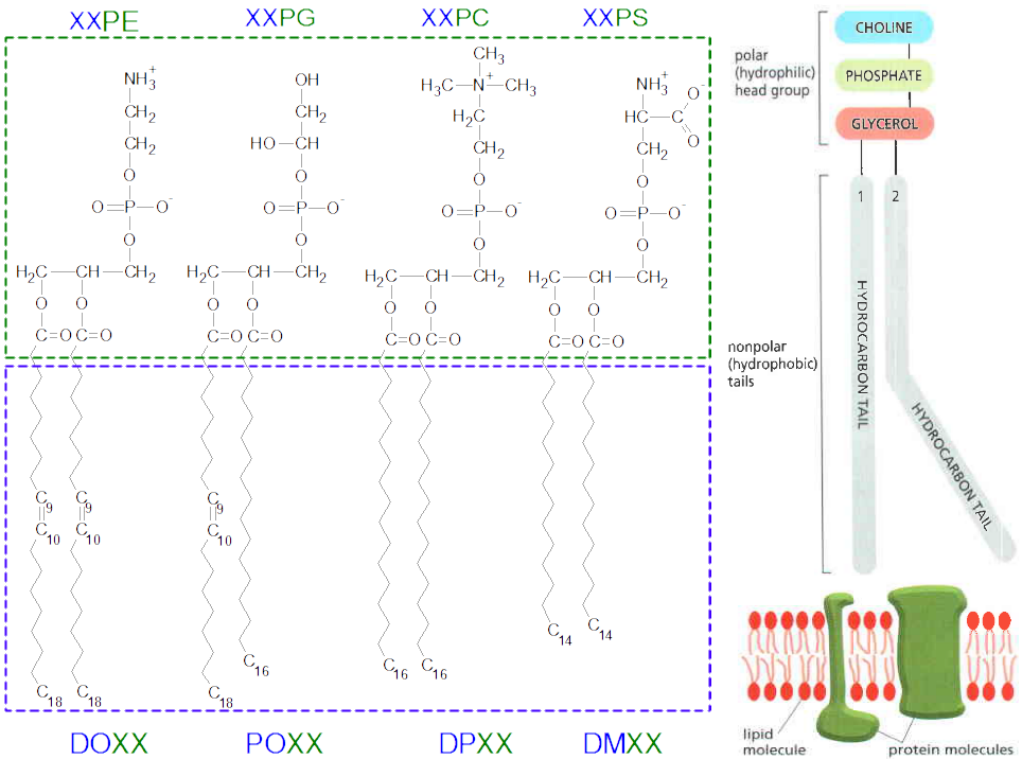

Figure 2.1.: (A) Some of the most widespread phospholipids head groups derived from glycerol (green border: PE - phosphatidylethanolamine, PG - phosphatidylglycerol, PC - phosphatidylcholine, PS - phosphatidylserine [3, p. 590; 1]) with some exemplary fatty acid tails that appear in the E. coli membrane (blue border: DO - dioleoyl, PO - palmitoyl/oleoyl, DP - dipalmitoyl, DM - dimyristoyl [48]). (B) and (C) Schematic pictures of a phospholipid and a cell membrane. Figures (B) and (C) from [3, p. 584f.]).

resulting amphipathic nature of phospholipids, the lipids spontaneously form clusters in water to bury the hydrophobic tails into the interior. At the end the lipids group into spherical micelles or planar double membranes

2.1.2. Composition of the lipid membrane

The cell membrane is not a homogeneous structure, but a mixture of different kinds of lipids with additional components. The lipids differ in their composition of the head group and of the two fatty tails (see fig. 2.1 A). Further the lipid membrane presents other non-lipid components like proteins. This diversity in the membrane's components leads to different mixtures of lipids that can be found in different kind of cells [3, p. 585]. The difference between the composition of the membrane of

bacterial and eukaryotic, especially mammalian, cells is of particular importance for drugs which act on membranes. Although they differ in many aspects, two of the differences are especially remarkable for AMP's mode of action.
The bacterial membrane exhibits a significant content of negatively charged lipids like phosphatidylglycerol (PG) while eukariotic membranes consist mostly of neutrally charged components like phosphatidylcholine (PC) and cholesterol, so that bacterial membranes tend to be highly electronegative.
Further membranes also differ in the content of sterols: cholesterol in eukaryotic cells, ergosterol in fungal cells and no significant amount of any sterols in prokaryotic cells. Sterols contribute greatly to the fluidity of membranes and are also a potential target area for antibiotics which are believed to affect the selectivity of AMPs (see. [17, 67]).
For example the E. coli membrane consists of 79 % PE, 17 % PG (negatively charged) and 4 % others, while the liver cell plasma membrane contains 24 % PC, 17 % cholesterol, 7 % PE, 4 % PS (negatively charged) and 48 % others [48].

2.2. Antibiotics

The term antibiotics refers to all substances produced by microorganisms or by chemical synthesis which inhibit the growth of other microorganisms. For treatment of infections caused by bacteria and fungi they need to be highly toxic to the target organism, but must not harm the host organism. Normally antibiotics achieve this selectivity by acting on target areas that differ in host organism from target organism by structure or mode of action. The target area can be divided in five broad categories: ribosome, folate metabolism, chromosome, cell wall and cell membrane. Because the exact modes of action differ strongly, they can not be summarized.
For instance, polymyxins bind to the liposacharid molecules of the outer membrane of bacteria to disorder it and penetrate the cytoplasmic membrane. There it binds to phospholipids and disrupts the membrane causing irreversible leakage of cytoplasm. Other antibiotics act by inhibiting the synthesis of vital elements of the organism. Imidazoles and triazoles, for example, inhibit the synthesis of ergosterol leading to membrane instability, growth inhibition and cell death [32, p. 152ff.].

Resistance to antibiotics

Resistance to antibiotics already existed at the beginning of industrial production of antibiotics, but due to the availability of other antibiotics this did not play an important role. First in the 1970s and 80s the situation got problematic due to the emergence of multiple drug resistance.
The resistance of bacteria evolves during therapy, where bacteria with a resistance gene for the used antibiotic are naturally selected. This results in an increasing number of resistant and multidrug resistant bacteria.
The mechanisms of resistance are as diverse as the mechanisms of antibiotic effects, but they can be classified into four major groups: inactivation of the drug, alteration of the target, reduced cellular uptake and increased efflux of the antibiotic molecules. For example, some bacteria developed a resistance to the mentioned polymyxin through the addition of a 4-amino-4-deoxy-L-arabinose (L-Ara4N) moiety to the lipopolysaccharides of the bacteria, so that polymyxin does not bind to the lipopolysaccharides any more [32, p. 202ff.].
The only possibility to counteract antibiotic resistance is well-directed usage of antibiotics, although it can only slow down this process, and the development of new antibiotics.

2.3. Antimicrobial peptides

Antimicrobial peptides are part of the natural defence mechanisms of most multicellular organisms and show an antimicrobial effect against a broad spectrum of bacteria, fungi and enveloped viruses.

2.3.1. Classification of AMPs

AMPs are a large and diverse group of short peptides, which can be subclassified according to various criteria. But some AMPs belong to multiple groups, while other can not be classified in any group at all. Hence the boundaries between the groups, depending on the type of division, should be seen as a smooth transition [11, 52]. The following overview should be considered as a short introduction to AMPs.

Charge The cationic AMPs (cAMP) are positively charged and show particularly strong interactions with negatively charged membranes of the bacteria. Also anionic

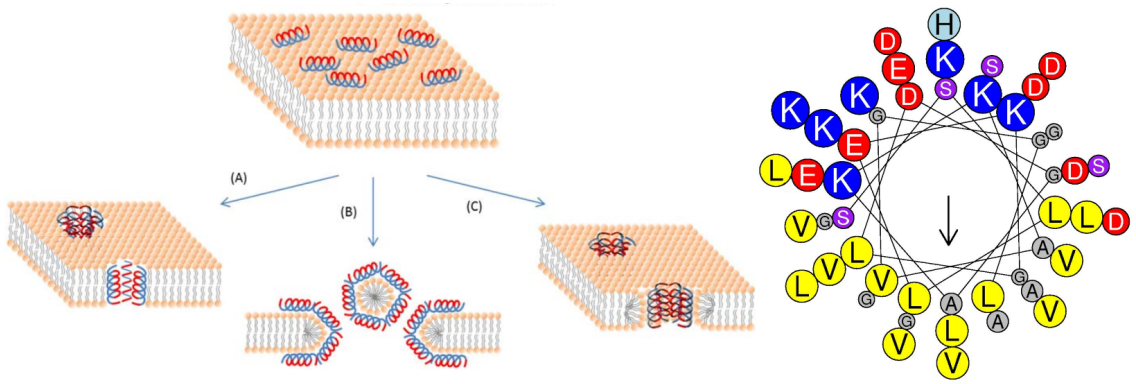

Figure 2.2.: (A) The three most common modes of action of AMPs: barrel-stave-, carpet- and toroidal-model. (B) Helical wheel diagram of dermcidin (colors: yellow - non-polar, purple - polar, red - negative charged, blue - positive charged, light blue and grey - others). The arrow points in the direction of the mean hydrophobic moment (see section 2.3.2). Figures from [7, 23].

AMPs (aAMPs) can be found in the nature. They act against both positively and negatively charged membranes, although aAMPs always have a negative charge. Moreover aAMPs, unlike cAMP, are active over a wide pH range [52].

Structure The most frequently forms are: β-sheet, α-helix, unfolded proteins and β-fold, whereas the peptides in β-sheet and α-helix form show higher antimicrobial activity [54].

Mode of action Many peptides attack the cell by penetrating their membranes: first the peptides bind to the membranes and align parallel to it. At higher concentrations the peptides start to cluster together and penetrate the membrane [5]. In the figure 2.2A the three most important possibilities of membrane penetration are listed [52].
The result is an uncontrolled exchange of ions between the cytoplasm and the cell's environment, so that the vital ion gradient between the cell interior and exterior is changed. This leads to loss of membrane-coupled respiration and ultimately to cell death. Although it is proven that some AMPs kill bacteria and disrupt the membrane, while other functions of this AMPs could not be found, it is not proven yet that membrane permeability is the only mechanism of the reviewed AMPs that kills bacteria [67].
Some peptides act through intracellular interaction: in this mechanism the AMPs combat microorganisms in a manner similar to the traditional antibiotics.

However, the dynamics of the interaction of AMPs with membranes is still understood poorly and leaves much room for speculation [7], so that the particular mechanism of action of the peptides can not be determined directly based on the belonging to a group.

2.3.2. Structure-activity relationship

In search of possibilities to increase the activity of AMPs and synthesizing new ones some publications chose to use an experimental approach to determine the relation between the structure and activity of AMPs. The result is a collection of properties that can be affected by mutation of amino acids and have a direct influence on the antimicrobial activity. The following section is a short overview of the results from [68] and concentrates on α-helical AMPs.

Size α-helical AMPs need to have a minimum length of about 12 residues to be able to form a stable α-helix with well defined hydrophobic and hydrophilic sectors. Other sorts of AMPs, like cyclic AMPs, show antimicrobial effect having only 6 residues.

Charge The most AMPs are cationic and interact through electrostatic and secondly through hydrophobic interactions. They have predominantly a positive net charge of 2 - 9 e, while a higher charge seems to disturb the helical formation.
Anionic AMPs interact with the mostly negatively charged membranes indirectly through electrostatic interactions involving divalent metal cations and through hydrophobic interaction. Because of this fact a high negative charge could prevent the aAMPs from interacting with the membrane.

Helix formation/Stability Although the stability of the helix is needed for a well formed hydrophobic sector, it seems that it does not improve the antimicrobial effect considerably. Instead it affects the haemolytic activity, so that it could be advantageous to decrease the stability of the helix to get a less toxic peptide. Various methods for estimating the stability of proteins are available. One possibility is the instability index (II) from Guruprasad et al. which has a range from 0 to 100 and indicates that a protein should be stable if the value is smaller than 40 [25].

The authors discovered that the stability of a protein depends on the dipeptides (compound of two amino acids) that are found in the protein. They assigned a weight value (DIWV) of instability to each of the 400 different dipeptides, so that II can be calculated by $\mathrm{II} = (10/L)\sum_{i=1}^{L-1} DIWV(x_i x_{i+1})$, where L is the length of the amino acid chain and $DIWV(x_i x_{i+1})$ the weight value of the dipeptide $x_i x_{i+1}$ with the starting point i on the amino acid chain. For calculating of II of of the various online tools can be used (for example [65]).

Amphipathicity An amphipathic α-helix possesses a hydrophilic site which faces the lipids while the peptide is lying on the membrane and a hydrophilic site which is aligned toward the water. The optimum value for an AMP is to have a hydrophobic sector that allocates 140-200 degree on a helical wheel projection (corresponds to $40 - 60\,\%$ content of hydrophobic residues). This property is needed for the AMP to be able to align on the membrane (see 2.2 B as an example).

Mean hydrophobic moment $\langle \mu_H \rangle$ The hydrophobic moment is the vectorial sum of all amino acid hydrophobicities which is normalized to an ideal helix: $\langle \mu_H \rangle = |\Sigma_{i=1}^{N} \vec{H}_i / N|$, where H_i are the hydrophobicities (various hydrophobicity scales are available, for example [21]) and N is the number of residues in the helix [19]. Increasing the hydrophobic moment results in a significant increase in the permeability of non-negative membranes and haemolytic activities.

Hydrophobicity H The hydrophobicity can be described as a non-vectorial sum of the hydrophobicities. This value has a similar meaning as $\langle \mu_H \rangle$. It describes the strength of the interaction with phospholipids. At the end the effect of the binding to the membrane highly depends on the hydrophobicity of the membrane, which implies that H is an important value for the selectivity of AMPs [67].

All these properties are indicators of antimicrobial activity but in the end the peptides have to be tested in vivo on different bacteria and blood cells to measure the minimal inhibitory concentration (MIC) and accordingly percentage rate of the hemolysis.

2.3.3. Resistance to AMPs

Although AMPs aim for a very fundamental component of the bacteria cell, these harmful microorganisms also developed resistances to AMPs. While some bacteria add positively charged amino acids to the membrane as a mechanism of resistance to cAMPs, there is no a simple method like this, that bacteria could use to resist aAMPs. Anionic AMPs interact with negative and positive membranes. aAMPs use the amphipathic nature of membrane lipids to interact with them which is a fundamental property of them and cannot be changed.
But there are still other possible mechanisms of resistance like degeneration or inactivation of the AMPs. For example, the bacteria Haemophilus influenzae can forward AMPs to the interior of the cell to degenerate them. In addition bacteria can try to make their membrane more stable, so that AMPs can not penetrate the membrane as easily [41].

2.4. Dermcidin

Dermcdin is produced in sweat glands and consists of 110 amino acids. The actual AMPs are produced in sweat from dermcidin by proteolysis. The longest AMP, that also shows the greatest antimicrobial effect of all produced AMPs and occurs most often on the human skin, is called DCD-1L and consists of 48 amino acids. It is an aAMP with α-helical structure, which acts through Barrel-Stave-Model [34].

2.4.1. Properties and advantages of DCD-1L

DCD-1L shows antimicrobial activity against a wide range of bacteria and fungi, such as Staphylococcus aureus, E. coli, Enterococcus faecalis and Candida albicans. The concentration of 1-10 mg/ml, which is found in sweat, already shows this effect. The advantages of DCD-1L, compared to other AMPs, is a wider range of efficiency, which covers the whole pH-range of sweat and is also conserved in solutions with s high salt concentration, as in sweat. This fact implies that dermcidin acts in a different manner than the so far known AMPs [52].
Human sweat is composed of eccrine sweat with a pH value of 5 to 6 (in some literature also a value of 4 to 6 pH can be found, for example [57, p. 138]) and apocrine with a a pH value of 6 to 7 pH [10, p. 910]. As dermcidin is produced in eccrine sweat glands, where also eccrine sweat is produced, it is possible that it acts

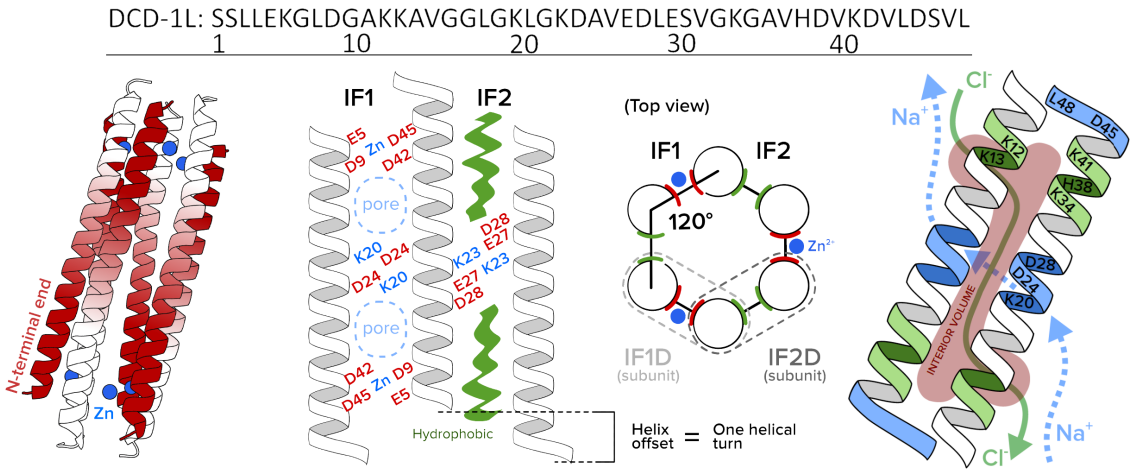

Figure 2.3.: (A) Amino acid single-letter code of DCD-1L. (B) The structure of the hexamer composed of anti-parallel aligned DCD-1L. The figure (C) illustrate the position of Zn^{+2} ions and the pores on the IF1 subunit from the side view, while the figure (D) visualize the position of the IF1 and IF2 subunits. (E) The ion path for cations and anions through the channel estimated by simulations. Figures (B)-(E) from [22].

mainly in slightly acidic sweat.

2.4.2. Structure of DCD-1L

Jung et al. were able to determine the structure of DCD-1L by using nuclear magnetic resonance (NMR) [34]. The research group used circular dichroism spectroscopy (CD-spectroscopy) to determine the state of DCD-1L in different solutions. In a 50 mM sodium phosphate buffer DCD-1L is present in disordered form, while in 20 mM sodium dodecyl sulfate (SDS) solution and in 50 % Triuormethanol (TFE) solvent it can be found in helical form.

DCD-1L consists of a flexible part around the N-terminus and a relatively ordered part around the C-terminus. The ability of the peptide to bind to the bacterial membrane is given by the amphipathic helical structure of DCD-1L. The charge of -2 and the acidic pI (isoelectric point) value of 4.89 does not disadvantage the interaction with the lipid membrane [29].

Another study by Song et al. in 2012 dealt with the structure of the ion channel that is formed by the individual DCD-1L peptides [61]. The research group could determine the structure of the ion channel with a resolution of 2.5 Å by using x-ray and other methods. They identified the structure as a hexameter formed by anti-

parallel oriented helices with a size of about $8 \times 4\,\text{Å}^2$. Each monomer forms two different areas with its neighbours: IF1 with $520\,\text{Å}^2$ that is stabilized by 2 Zn^{+2} and IF2 $930\,\text{Å}^2$ that exhibits two holes with a diameter of 1 nm each.

2.4.3. Mode of action

With the knowledge of the structure of the ion channel and additional tools, such as electrophysiology and molecular dynamics simulations, the research group Song et al. could investigate the interaction of DCD-1L with lipid structures. The simulation of dermcidin in a bacteria-like (POPE/POPG, 3:1) double membrane showed an inclined position of the ion channel within the membranes (30°), an unexpected path of the ions through the side holes in the IF2-surfaces and unobstructed water flow through the channel.
Later B. Forsberg showed in his master thesis the independent path of cations and anions inside of the ion channel by using simulations (see fig 2.3D) [22]. Assuming ohmic behaviour he estimated the conductance to $(62.5 \pm 7.6)\,\text{pS}$ (in a 0.15 M NaCl solution with a potential of 0.5 to 0.9 V), which agrees with the experimental value of $(81 \pm 14)\,\text{pS}$ reported by Song et al. (in a 1 NaCl solution with a constant 0.1 V potential). Another publication with experimental results for the conductance of dermcidin for different potentials reported evidence for non-ohmic behaviour and a conductance of 20 to 151pS in the range of 10 to 100 mV [52].
No reports about other modes of action of DCD-1L could be found in literature, although it is possible that they are yet not identified.
While dermcidin shows a wide range of antimicrobial activity, the bacteria Staphylococcus epidermidis, which is considered a normal part of the human skin flora, was identified as resistant to a large number of antibiotics and also to dermcidin. Usually S. epidermidis does not pose danger to humans, but it can cause dangerous infections in people with low immunity. The bacteria raises extracellular proteolytic activity to degrade dermcidin. These mechanisms explain why dermcidin and S. epidermidis cohabitate on human skin [40].

3. Methods

3.1. Molecular dynamics (MD)

Molecular Dynamics (MD) is a computer simulation of atoms and molecules where the spatial trajectories of particles are calculated using numerical methods. The trajectories are determined by Newton's equation of motion.
MD offers many advantages, like filling the gap between theory and experiments, where theory is too complicated to be applied on a given system. It can also be used to achieve high resolution insights when experimental resolution is not sufficient.
The most accurate and reliable method to calculate the forces between particles is by using quantum mechanical (QM) equations. Although approximation methods like Hartee-Fock (HF) methods are used, QM MD is only a possible options for small systems with a few hundreds particles in a time scale of hundreds ps [49].
Often, especially in biophysics where systems with more than 100.000 atoms are common, molecular mechanics (MM) which uses classical mechanics to model molecular interactions is used. In MM all particles are assumed as spheres with the corresponding van der Waals radius and the forces are calculated by using potentials, which consist of different terms for interactions between bound and non bound atoms. The contributions for non bonded interaction are described by the Lennard-Jones potential, that combines potentials from Pauli repulsion and the van der Waals force, and electrostatic interaction, while bonded interactions are calculated using functions from classical mechanisms like the potential between two particles depending on bond length, bond angle and torsion angle like in the figure 3.1. The parameters that are needed for MM are called forcefield and need to be fitted to experimental results. Later on in the simulation no fitting of these parameters is allowed.
An important property of MD are the boundary conditions. Most simulations in biological systems use a periodic boundary conditions (PBC): if a particle leaves the simulation box on one side, it reenters in the box on the opposed side. In this manner an infinite system can be approximated by a small one [49].

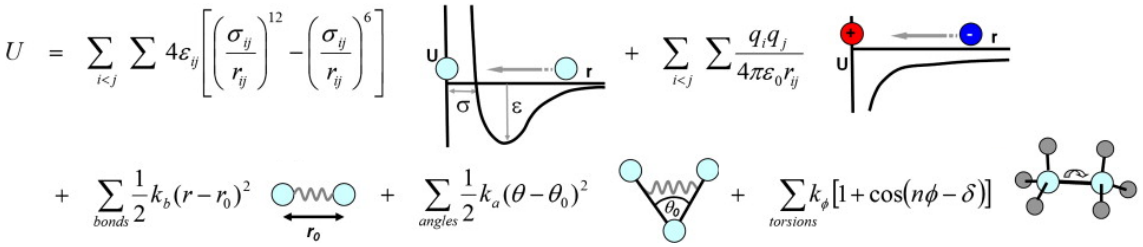

Figure 3.1.: An Example for the terms that contribute to the potential, that is needed to calculate the Force in MM. The contribution for non-bonded interaction are described in the upper line by the Lennard-Jones potential and electrostatic interaction. The lower line shows exemplary potentials that are used to describe the potential between two particles depending on bond length, bond angle and torsion angle. Figure from [50]

3.2. Computational electrophysiology

To simulate the properties of an ion channel inside a membrane a transmembrane voltage (TMV) is needed. This can be achieved by applying external voltage or creating two components with different ion concentrations. C. Kutzner et al. decided to use the second option to perform realistic simulations of ion flux through channels by using the electrochemical gradient. In the computational electrophysiology (CEP) setup the simulation box is divided in two compartments α and β by two membranes (see figure 3.2). Because a charged system could introduce artefacts (see ref [31], the net charge of the whole box has to be neutral. A voltage difference between compartment α and β can be achieved by a small charge imbalance between these compartments.The resulting voltage can be calculated by double integration of the charge density. To sustain a constant ion concentration in both compartments an exchange algorithm for ion/water pair was implemented, which counts the ion in both compartments in a given interval,. The resulting voltage could be determined by assuming that the membranes form a capacitor. Thus it is possible to apply the formula $\Delta U(t) = \Delta n(t)\mathrm{e}/\mathrm{C}$, where $C \approx 1\mu\mathrm{F/cm}^3$ is the capacity of a lipid membrane [58], e the elementary charge and $\Delta n(t)$ the difference of the ions between compartments α and β [38]. In praxis the adsorption of ions by charged molecules can lead to a different mean value of ΔU while stochastic fluctuation in the charge density let the voltage difference vary within a single run of simulation.

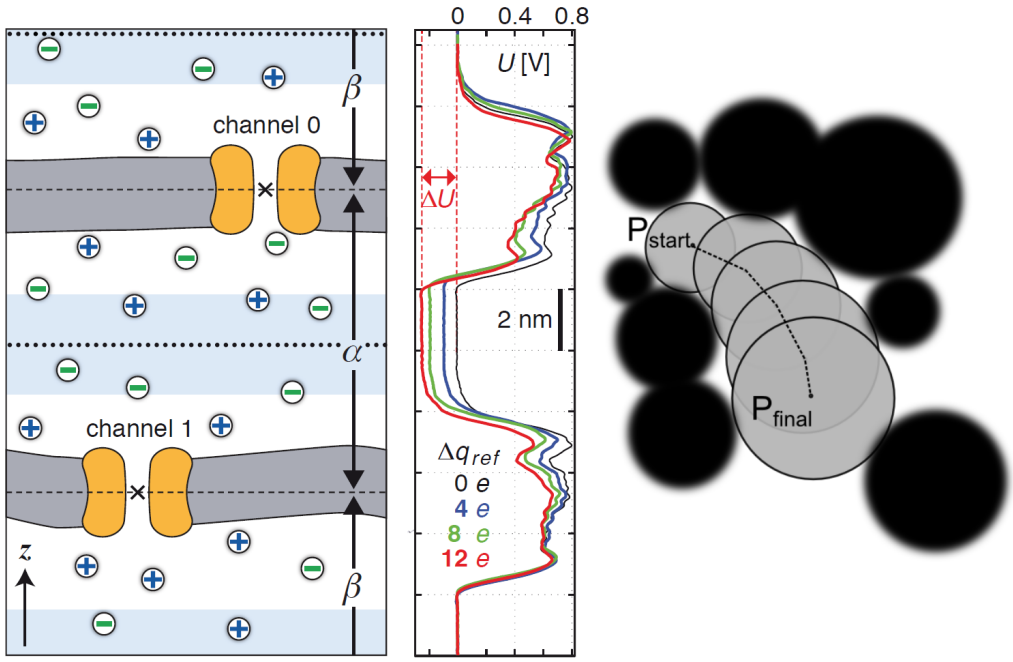

Figure 3.2.: (A) Schematic view of the simulation setup: grey - lipid bilayers, orange - ion channels, green - anions, blue - cations, dashed lines - boundaries between the compartments α and β, dotted lines - compartment mid-planes. (B) Exemplary electric potential plot averaged over 50 ns: x-axis - electrostatic potential U, y-axis - coordinates like the y-axis in figure A, line color - different charge imbalances. (C) Schematic explanation of HOLE: the algorithm needs a starting point P_{start} inside the channel to maximize the radius, which is allowed by the van der Waals radii of the surrounding atoms and yields the center of sphere P_{final}. Figures (A) and (B) from [39]

3.3. HOLE

For measuring the radius of the channel the software HOLE is being used [60]. This software uses a Monte Carlo algorithm to find the centre of a sphere with the maximum radius (see figure 3.2 C). To accomplish this HOLE needs a starting point inside the channel and a vector which points in the direction of the channel. The search is only performed on planes normal to the channel direction vector whereby the distance between the planes is given by the user. Besides the path and the radius of the channel the residue which is nearest to the center of the sphere with the maximal radius is also put out. Although theoretically as many as three points are needed to define the radius and center of a circle in a plane, only one of them is determined as the closest one because of machine precision.

As HOLE was developed to measure the radius in the main channel and only mu-

tations concerning the main path of the channels were made, here only the radius profile of the cavity alongside the z-axis was explored.

3.4. Detection of functional modes

3.4.1. Principal component analysis and functional mode analysis

Functional motion is often involved in the mode of action of proteins. This motion can be studied in MD but frequently it can not be associated with the function due to big random fluctuations of the molecule. In other words: the configuration space of the space is too big. To associate the functional dynamics with the real motion of the protein first a dimension reduction is needed.
One possible solution for this problem is principal component analysis (PCA), which reduces the proteins' configuration space by determining a set of vectors with the largest contribution to the mean square fluctuation of the protein. For this purpose the covariance matrix C with the matrix elements $C_{ij} = \langle (x_i - \langle x_j \rangle)(x_j - \langle x_j \rangle) \rangle$ for the system with $x_i(t)$, where $i = 1, ..., 3N$ and N is the number of particles, is calculated. After diagonalization 3N eigenvectors e_i with the eigenvalues σ_i^2 are obtained. The eigenvectors are sorted according to descenting fluctuation which is equal to the eigenvalues σ_i^2. The resulting projections $p_i(t) = [x(t) - \langle x \rangle]e_i$ are called principal components (PCs) [30].
For the further analysis only the first 10-20 eigenvectors, which normally contribute $80 - 90\%$ to overall motion, are used. While having a reduced configuration space functional mode analysis (FMA) can be used to detect the motions that are maximally correlated to a given observable, for example a chemical or geometrical one like the radius of a channel. By using the eigenvectors from the PCA as a new basis a motion that has the maximal correlation with the observable can be calculated.

3.4.2. Partial least-squares functional mode analysis

The fact that some FMA applications need a higher dimensional basis than other reveals that the PCA basis does not always provide the ideal solution basis for FMA. The basis from PCA was only chosen to explain the motion of the protein and not the observable. To overcome this issue partial least-squares FMA (PLS FMA) was developed. PLS is a regression method that has some similarity to principal

component regression which is based on PCA and standard linear regression. In contrast to PCA, PLS also uses the correlation between the coordinates and the observable to calculate the basis iteratively. Let $\mathbf{f}$ be a vector of n observables and $\mathbf{X}$ an $n \times p$ matrix of p coordinates. The purpose of a regression is to find a p-dimensional coefficient $\boldsymbol{\beta}$ for the relation $\mathbf{f} = \mathbf{X}\boldsymbol{\beta} + \boldsymbol{\epsilon}$ with the error $\boldsymbol{\epsilon}$, which should be as small as possible. PLS constructs at every step a new set of k regressors $\mathbf{T}_k$ as a linear combination of the original coordinates $\mathbf{T}_k = \mathbf{X}\mathbf{W}_k$ so that all $\mathbf{T}_k$ have the maximal covariance with $\mathbf{f}$, while $\mathbf{T}_k$ is uncorrelated to each previous coordinate in $\mathbf{T}_k$. This iteration (also called training) will lead to a basis of vectors that optimally describe $\mathbf{X}$ and $\mathbf{f}$ [16].

The optimal number of the regressors $\mathbf{T}_k$ is not known in advance and has to be estimated by using different values for k and performing cross-validation of the results.

PCA-based FMA does not use the entire trajectory of the protein for the modelling but only half of it. So the quality of FMA can be measured through cross-validation with the correlation between the model and the data that was not used for training the model [37]. In this study PLS FMA was used to determine the motion of the protein that is involved in the change of the radius. If a gating mechanism is present, a stabilization of the open state of the channel could also lead to better conductances. Due to this reason the channel is also analysed for gating mechanism.

As input three simulations with a total time 1.2 of µs of a single DCD-1L channel in a bilayer membrane without TMV which was performed by Chen Song[1] were used. Because residues at different positions could change the radius independently from each other, the channel was divided into eight sections with a length of 5Å and FMA was used independently on all of these parts. Thus only the region ± 20 Å around the center of mass of the channel was analysed for gating relevant motion. The coordinates of all atoms of the protein except hydrogen ($p = 1980$) from 11715 frames ($n = 11715$) were used as the coordinates $\mathbf{X}$ and the minimal radius of the channel from a given section, which was measured by HOLE, was used as the observable $\mathbf{f}$. For determining the number of regressors $\mathbf{T}_k$, FMA was performed with different number of regressors and the value of k was chosen as the correlation coefficient between the model and the data which was not used for PLS FMA (another 11715 frames) to be at least 98% of the maximal correlation, while having the smallest number of regressors. For estimating the significance of the correlation coefficient

[1]Now at Dept. of Biochemistry, University of Oxford.

the bootstrapping method which is based on random sampling with replacement was used (for further details see ref. [18]). The correlation coefficient between 10^5 resampled datasets and the model data of each compartment was calculated to estimate a p value for different correlation coefficients. As the data points are correlated, only every 20th data point (586 data point per section, one data point per 2 ns) was used. This leads to less correlated data points and an increase of the p value for a given correlation coefficient, as less data points for its calculation are used.

3.5. Essential dynamics

The functional motion of proteins often includes large changes in the configuration space of the proteins. This usually means that proteins need to be simulated long enough to explore the relevant part of the configuration space of the examined object. A. Amadei et al. invented a method called essential dynamics (ED) analysis that, among other things, should also improve the sampling efficiency [4]. It uses constraint forces to sample the configuration space along some collective coordinates (eigenvectors). Various options for driving the system along a vector are available (see ref. [2]). It is also possible to fix the structure at a given point of a vector by applying a potential that produces an attractive force.
To analyse the conductance of the channel as a function of the value of the projection of a PLS FMA vector, 18 ED simulations were performed. Each simulation consists of 20 ns equilibration and 80 ns main run a. The simulations were performed using the system for CEP simulations, as described in section 3.7, but additional changes had to be made. To measure the conductance at 6 different values of the projections, a constant quasiharmonic restraining potential, which keeps the values of the projections constant at a given value, was used. The parameter $Eflnull$, which is the force constraint of the restraining potential, was set to 1000 kJ/mol nm.
Although the simulations could be started with a system that has any projection of the eigenvalue, the first attempt has shown that a fast changed of value of the projection of the PLS vector can lead to a deformation of the protein. To solve this issue two additional 10 ns ED simulations were performed: one at which the value of the projection was slowly changed to the maximum desired value of the projection and a second one where the projection was changed from the maximux to minimum value. Six snapshots at different values of the projection that should be sampled

were taken from the second simulation and were used as the start configurations for the proper ED runs.

3.6. Mutants

The mutations are made to analyse the conductance in relation to changes in the channel radius and charged residues inside the channel, whereupon the final aim is a mutant with increased conductance. Furthermore the mutations are made respecting the properties of DCD-1L as an aAMP.

3.6.1. Improvement of conductance

The simplest prediction of the channel conductance can be made by ohmic law assuming that the channel is filled with an electrolyte. The conductance depends on the resistance of the electrolyte, the cross section and length of the channel [28, p. 351]. The resulting conductance is not realistic, but it can be assumed as an upper limit that is set by the dimension of the channel. Furthermore the radius is assumed to be one of the most important properties of the channel that can influence its conductance. The channel radius can be increased by changing long residues which extend into the channel to shorter ones.
To see if the conductivity is influenced by charged residues, the residues can be mutated to neutral residues of the same length. Long charged residues could repel ions and prevent them from passing through the channel.
The radius profile is often not static but can vary from a small radius which makes the channel impassable for ions to an open state. This behaviour is called gating. The most common mechanism of gating in biology is reducing the radius by motion of a large part of the protein or by the motion of a single side chain [28, p. 617f.]. The gating behaviour can be influenced by different signals, like binding of a ligand to the channel (for example the Cys-loop receptors [14]) or a change in the TMV (like the voltage-dependent K^+ channels [43]).
Also other factors can influence the conductance, but as long as there is no evidence that these play a big role, no further investigation in this direction will be made.

3.6.2. Conserving functions as AMP

Due to the importance of the N- and C-terminus for the interaction with the lipid bilayer, no truncated DCD-1L were analysed in this study. Although B. Forsberg already demonstrated that truncated DCD-1L exhibits an improved conductance [22], there are experimental results that show that these have lower antimicrobial effect [55]. A DCD-1L derived peptide with only the first 47 of 48 residues, without the last C-terminal leucine, shows a three-fold smaller affinity to a POPC:POPG membrane [34].
As the hydrophobic effect, which is responsible for the grouping of hydrophobic substances in solutions, is crucial for the antimicrobial effect of dermcidin, the hydrophobic moment should not be reduced by putting a hydrophilic amino acid in the hydrophobic sector.

3.6.3. Investigated mutations

To test the dependence of the conductance on the charge or rather if the conductance stays the same for the same radius, four combinations of the residues K23 , E27 and K34 were mutate to glutamine, which is a natural neutral hydrophilic amino acid. Although it is the longest hydrophilic uncharged amino acid, it has one C-atom less than lysine and is thus shorter. On the other side, glutamine has the same number of carbon atoms as glutamic acid but glutamine is slightly bigger because it ends with an NH_2 and not a single oxygen like glutamic acid.
The mutants **E27Q**, **K23QK34Q**, and **K23QE27Q**[2] were created to see the dependence of the conductance on the charged residues. As the residue K34 is not protonated, the mutant **K23QE27QK34Q** should give the same or slightly better results as K23QE27Q.
Three mutants were generated to see the influence of a smaller radius on the conductance. For this purpose, among others, the non-natural amino acid diaminybutyric acid (Dab), which is derived from lysine and shorter than lysine and histidine [24], was used. The two mutants **K23HE27D** and **K23DabE27D** exhibit residues with the same charge as WT, but as histidine/dapamine is shorter than lysine and aspartic acid shorter than glutamic acid, these two mutants should show bigger radii. Also one mutant **K23SK34S**, where the two long charged amino acids were changed

[2]Nomenclature: XNY - the amino acid X on position N is mutated to the amino acid Y. In case of multiple mutations in one peptide, the terms are stringed together.

Mutant	Δr	ΔQ [e]	Mutant	Δr	ΔQ [e]
E27Q	-	+6	K23DabE27D	yes	0
K23QE27Q	-	0	K23HE27D	yes	0
K23QK34Q	-	-8	K23SK34S	yes	-8
K23QE27QK34Q	-	-2	A11LA14LK23QE27QK34QA34L	-	-2
A11LA14LK23QE27QD28VK34QA34L				-	-1

Table 3.1.: Overview of the tested mutants. The column Δr indicates if the mutant should have a reduced radius and the column ΔQ gives the change of the net charge of the mutant compared to WT in the used protonation state.

to two short neutral ones, was created.
On the basis of K23QE27QK34Q two other mutants, where additional changes concerning the mean hydrophobic moment $\langle \mu_H \rangle$ and hydrophobicity H were made. The alanine residues which have the hydrophobicity $H_A = 0.310$ at the positions 11, 14 and 36 were changed to leucine with $H_L = 1.7$. Due to the resulting long name using the standard nomenclature, this mutation will be refereed as **QQQLLL**. Furthermore on the QQQLLL mutant the residue D28, which has a hydrophobicity of -0.770, was changed to valine with $H_V = 1.220$. Although this is a mutation of a hydrophilic to a hydrophobic residue, it does not change the hydrophobic moment of DCD-1L considerably because the hydrophobic moment of D28 is perpendicular to $\langle \mu_H \rangle$ (see figure 2.2 B). Beyond that, this mutation will increase the mean hydrophobicity. As four of the six residue D28 are protonated, this changes the net charge only by +2 comparing to QQQLLL. In the text this mutation will be called **QQQVLLL**. An overview of the mutation can be found in table 3.1

3.6.4. Protonation state

In most of the simulations an alternative protonation state that was calculated by Chen Song and should yield the protonation state of the channel at a pH value of 5 was used (see appendix A.1). The calculations were performed using MEAD which determinates the protonation state of molecules based on the Poisson-Boltzmann-equation [6]. Due to the lack of confirmation of this protonation state by other methods, this state was not used in simulations until now. Other methods like the empirical method PROPKA [56] produced different protonation states. Although this state is not proven, it is a theoretical possible option that can lead to new results and show, if the conductance of dermcidin depends on the protonation state .
To see if the protonation state can influence the conductance simulation runs of WT

and K23QK34Q with default protonation state were also tested. The proteins with the default protonation states will be denoted with the index „DP“

3.7. Parameters of the simulation

For all simulations the GROningen Machine for Chemical Simulations (GROMACS) 4.6.5 [27, 64] software package and the forcefield CHARMM36 (C36) were used [36]. C36 is an updated version of earlier CHARMM FF with a more realistic performance of phospholipide bilayers (for further informations see references).
For the start system, which is adopted from C. Song, first a bilayer of 72 POPE and 24 POPG (POPE/POPG, 3:1) was made with the CHARMM-GUI [33] and then equilibrated in GROMACS. The dermcidin ion channels (PDB ID: 2YMK) were inserted into the bilayers using the GROMACS tool g_membed by removing nine lipids [66]. This system was equilibrated again and normal simulation runs under NPAT conditions which conserve the number of particles (N), pressure (P), surface area of the lipid membrane (A) and temperature (T) were started. For performing CPE the single channel system was duplicated, concatenated in the z-direction and equilibrated for 1 ns. For further details on the making of the start system see supporting material of Song et al. [61].
All mutations were performed on the system described above using PyMOL with the „SwissSidechain - PyMOL Plugin“[24, 59]. The resulting simulation box has a dimension of $7.68 \times 7.68 \times 22.62\text{nm}^3$ and contains a (1.0 ± 0.1) M solution of NaCl composed of ca. 27015 ± 15 water molecules and ca. 940 ± 12 Ions (Na/Cl, ca. 58:42). Because the simulation box has to be neutrally charged, the exact number of water molecules and ions depends on the charge of the mutant. After the mutation a short energy minimization using the steepest descent algorithm with 1000 steps and a short equilibration run with a length of 4 ns (with the same parameters as the main simulation) was applied.
All simulations were performed using virtual sites model for hydrogen atoms which allows to use of a 4 fs time step [35]. The neighbour list was handled by the Verlet list with a cut-off of 1.3 nm which was updated every 50 steps [51]. Electrostatic interactions were treated with particle-mesh Ewald (PME) method with a cut-off radius of 1.3 nm [20]. Van der Waals forces were calculated explicitly up to a distance of 0.8 nm and beyond this point switched off continuously smooth to zero at 1.3 nm. A Fourier grid spacing for PME of 0.15 nm was chosen.

The proteins together with the Zn^{+2} ions, lipids and water molecules were coupled separately to a temperature bath using the v-rescale method with a temperature of $T_{ref} = 310$K and time constant $\tau_t = 0.1$ps [13]. A semi-isotropic Berendson pressure coupling to 1 bar with a time constant $\tau_p = 2.0\,$ps was used, so that the size of the box was only adjusted in the z-direction [8]. The algorithm linear constraint solver (LINCS) using the 6th order was applied for all bonds [26].
The chosen molarity of 1 Mol NaCL and the transmembrane voltage (TMV) of about 0.6 V are higher than the physiological values (TMV: 50 to 140mV [67] and NaCL concentration in sweat 20 - 110 mMol [12, 47]), but allow a better sampling: using the physiological values would lead to a longer simulation. Also in experiments, like single channel conductance measurements [52], where no problems are reported the same molarity of 1 Mol is used. The only limitations for the TMV is the electroporation, the formation of pores due to externally applied potentials. Generally no electroporation occurs when less than 1 V voltage is applied. For example, for causing pore formation voltages in the range of 0.5 V/nm are reported [62].
The conductance was calculated using Ohm's law $G = R^{-1} = I/V$ by averaging the current I and voltage V over 20 ns.

4. Results

4.1. Radius profile

The radius profiles in figure 4.1 were calculated by using all simulated channels of a given mutant or protonation state. This means that one plot is made from 4 runs $\cdot 2$ channels/run $\cdot 160$ ns/run $= 1280$ ns . As the standard deviation for all plots varies about only 0.15 to 0.30 Å, they are not shown for most mutants on the graphs due to clarity.
Although the radius profiles should be symmetric, small differences between the two sides can be spotted. The centres of mass of both channels are shifted along the z-axis in negative direction by 2 to 8 Å with respect to the center of mass of the lipid bilayer resulting in structural differences between the two sides of the channels can be caused. The reason of this behaviour was not investigated, but due to the fact that no drift of the center of mass of the channels in the z-direction could be observed, it is assumed that the shifted position of the channels is a property of its equilibrated state.

Default and modified protonation state

While no differences in the radius profile of K23QK34Q and K23QK34QT$_{\mathrm{DP}}$ could be observed (data not shown), slight differences between WT and WT$_{\mathrm{DP}}$ exist. The profile of the WT has a by 0.4 Å bigger radius at $z = \pm 30$ Å. Inspecting the profiles of every single run reveals the reason: while the single runs of WT$_{\mathrm{DP}}$ did not show any anomaly and all profiles have the same shape, significant changes in WT runs of the radius at $z = \pm 30$ Å could be observed. Some channels exhibit two closed ends (a radius smaller than 2 Å), some of them one open and one closed, while one channel possesses a continuous radius bigger than 2 Å (see figure 4.2). Despite nearly the same radius profile, both mutants with default protonation state show a higher conductance (see section 4.5.1) than the alternative protonation state. Assuming

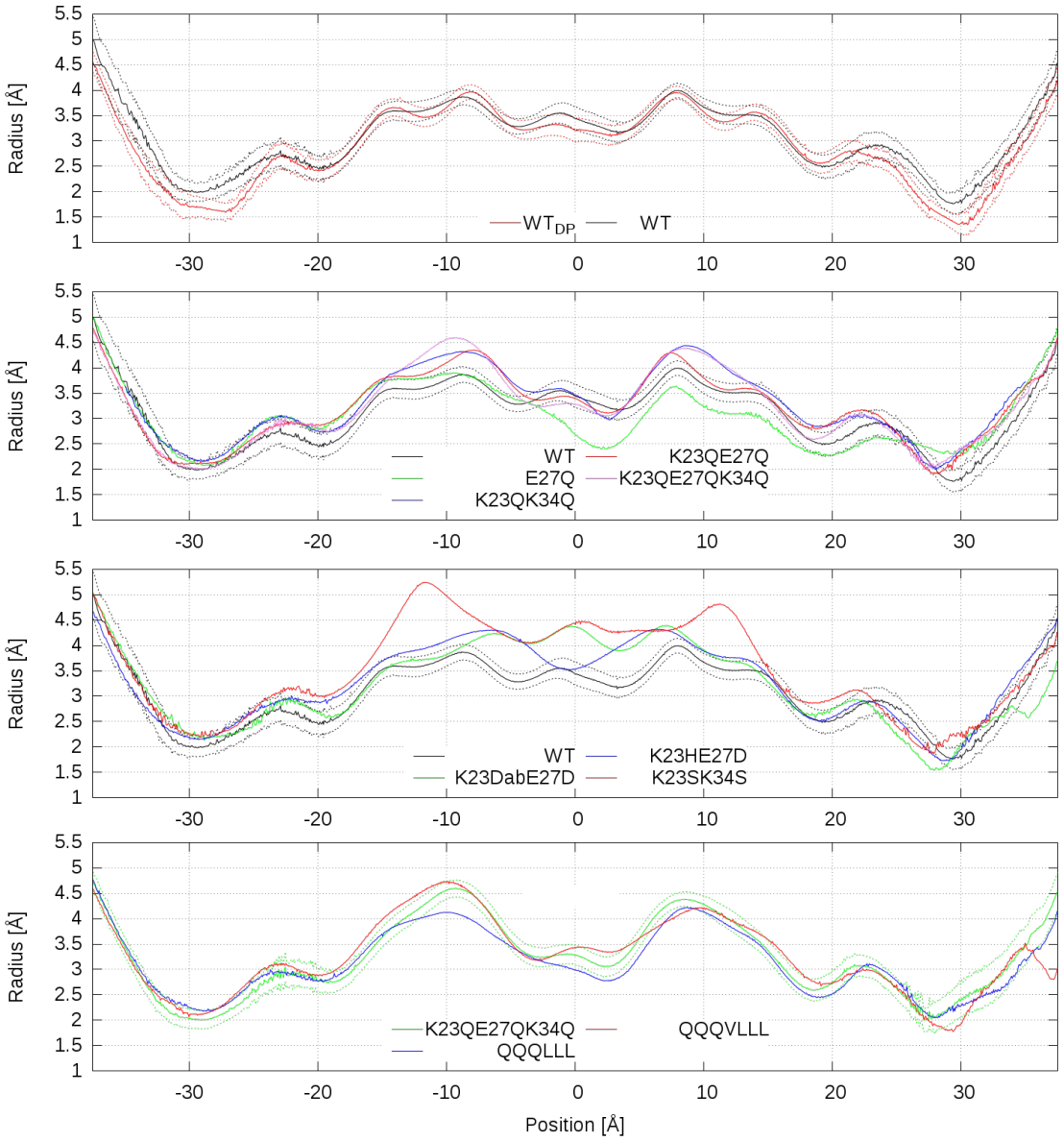

Figure 4.1.: The radius profiles for different mutants, averaged over simulated channels of a given mutant. The doted lines represent the standard deviation of the averaged radius profiles. The most standard deviations are nearly constant, so that they are not plotted for the most mutants.

that nature uses the optimal solutions, the default protonation state seems to be more realistic.

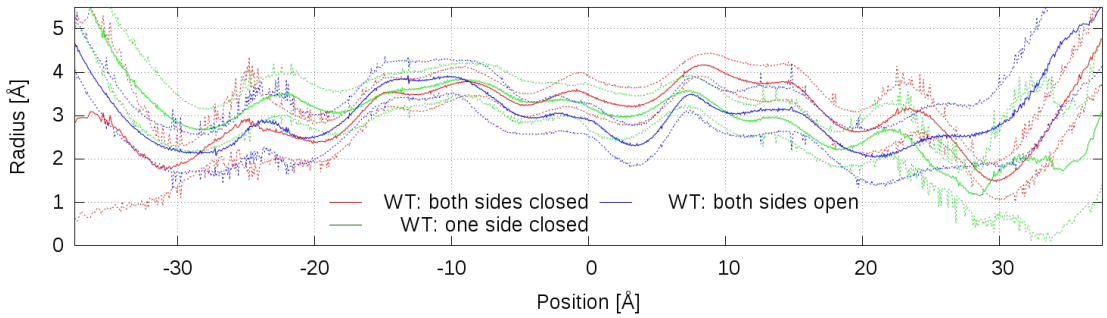

Figure 4.2.: The radius profile of WT averaged over one simulation from three different channels: red - closed on both sides, green - one side closed and one side open, blue - open on both sides. The dotted lines show the standard deviation

Mutants

The radius profiles for K23QK34Q, K23QE27Q and K23QE27QK34Q stayed mostly the same as the profile of DCD-1L. As expected, for the mutant K23QE27QK34Q the radius in the region near the residue K34 at $z = -9\,\text{Å}$ gets bigger by $\Delta r = (0.69 \pm 0.24)\,\text{Å}$. The expected length difference between K and Q can be estimated by using the length of a simple C-C binding $d_{C-C} = 1.52\,\text{Å}$ and the angle between three C-atoms in a sp^3 hybridization $\alpha_{C-C-C} = 120°$, which results in a difference of $\Delta d = \sin(\alpha_{C-C-C}/2) \cdot d_{C-C} \approx 1.2\,\text{Å}$. This calculation should be seen as a rough estimation of an upper limit. Also the change of the radius by $\Delta r = (-0.77 \pm 0.29)\,\text{Å}$ at $z = 5\,\text{Å}$ for E27Q can be explained in a similar way. Thus, glutamic acid ends with an oxygen atom, which has more or less the same van der Waals radius as the nitrogen in the amine at the end of the glutamine residue, but the amine contains also two hydrogen atoms with a radius of 1.1 Å [9].
Considering these two results, it is unexpected that the radius near K23 and near E27 in the case of K23QE27QK34 did not change as predicted. Two possible explanations are that also structural changes in the backbone take place or the sidechains are not pointed vertical to the z-axis to the middle of the radius, but are tilted to the side or up/down. This behaviour was observed for the opening/closing behaviour for WT (see section 4.3.2), but it was not investigated if the same mechanism leads to an increased radius of the mutants.
The mutants which should have an increased radius, changed their radius in the expected range. The mutation of lysine to histidine did not change the profile at all, although a small difference would be plausible. Even though no change of glutamic acid at position 27 was made, an $\Delta r = (0.98 \pm 0.30)\,\text{Å}$ increased radius at $z = 0\,\text{Å}$ for

K23SK34S can be reported. The explanation for this increased radius could be the same as mentioned above in the case of K23QE27QK34. At the end K23SK34S possesses the biggest average channel radius: the average radius in the range $z = \pm 15$Å was increased from $r_{Av,WT} = (3.54 \pm 0.20)$ Å to $r_{Av,K23SK34S} = (4.45 \pm 0.33)$ Å.
The changes concerning the AMP properties of DCD-1L did not cause serious changes in the radius profile for QQQVLLL, while QQQLLL manifests a decreased radius compared to K23QE27QK34. As the alanine residues which were changed to leucine residues are outside of the channel, the change of the radius is probably caused by an alteration in the backbone or in the oligomerization of the ion channel. This aspect remains for future research.

4.2. Permeation path

The investigation of the ion path in WT_{DP} reveals new insight compared with the model presented by B. Forsberg (see also figure 2.3 D) [22]. In 25% of the channels the Na^+ ions enter and exit through the pores at the residues K20, D24 and D28, but this path seems to play only a less significant role. In his master thesis Forsberg justified the Na^+ ion path by the increased interaction of the ions with the residues K20, D24 and D28. In the observed simulations mainly the remaining of Na^+ ions at these residues, not the permeation through the ion channel, could be observed. In 75% of the simulation only one of the pores near the residues K20, D24 and D28 was used either for entering or leaving. Instead, Na^+ ions use mainly the same pores as Cl^- ions and the openings at the channel termini.
In the simulation no fixed ion path, which was used in all simulations, could be seen, but the path appears to vary depending on the pores that are most easily accessible. Thus it is possible that the permeation path depends on the position of the channel relative to the membrane and on the tilt angle of the channel.
The observed path for Cl^- ions is mainly the same as stated by B. Forsberg: only few atoms penetrate the channel by the end openings while the bigger part use the pores at residues K34, H38 and K41.
In the alternative protonation state the ion path differs even more in the permeation path: while the path for Cl^- stays mostly the same as described above, the N^+ cations use in equal measure the end opening and pores near the residues K34, H38 and K41 to transit the channel. For no mutant a significant change in the permeation path could be observed.

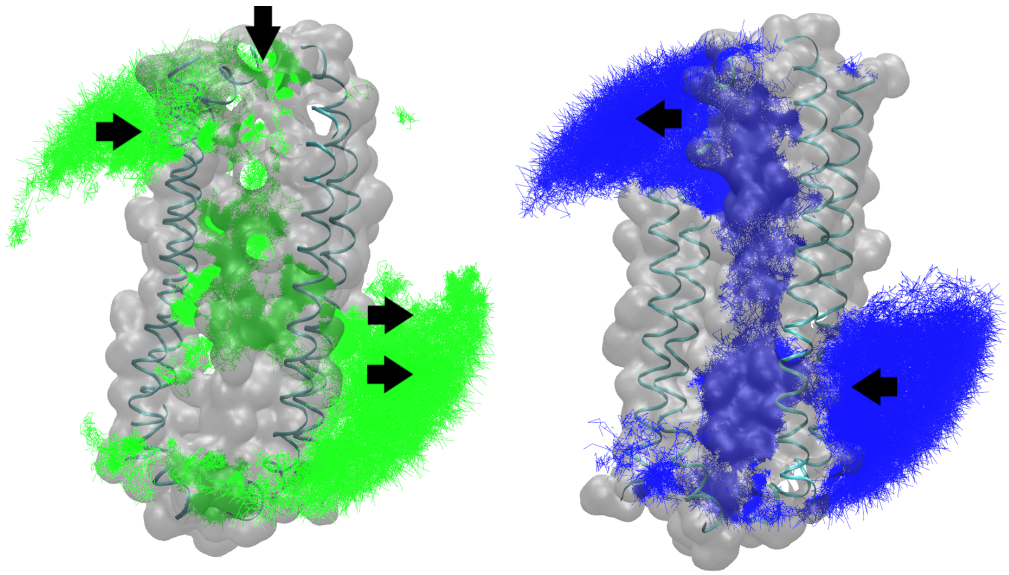

Figure 4.3.: Exemplary path of Cl^- (green) and Na^+ (blue) of the dermcidin channel with default protonation sampled over 160 ns. The arrows mark the observed entrance and outcome, which are representative for this and other WT_{DP} simulations. For clarity only four of six α-helices are shown.

4.3. Gating mechanism

4.3.1. PLS FMA

After performing PLS FMA for $k = 1, .., 30$ regressors $\mathbf{T}_k$, $k = 16$ was chosen for further analysis. Using HOLE and vmd for visual inspection both backbones and residues could be observed to be involved in changing the radius.
As can be seen in figure 4.4 the correlation coefficient in the region $-20\,\text{Å} < z < 15\,\text{Å}$ varies from 0.55 to 0.77 . To estimate the significance of these coefficients the p-values of the correlation coefficient $R_C = 0.02$ and $R_C = 0.05$ was calculated. For the data of each section the bootstrapping method was used and the average correlation coefficient for both correlation coefficients $p_{R_C=0.10} = 0.008$ and $p_{R_C=0.20} \approx 0$ (not achieved) were obtained. Thus the achieved correlation coefficient can be called very significant.
In figure 4.6 the motion of the backbone and residues Lys23, Glu27 and Lys34 can be seen: the backbones are bending outward while the residues turn sidewards and/or

up-/downwards. Thus not only the average radius gets bigger, but also the minima in the radius profile, that represent bottlenecks in the channel caused by the residues, disappear. This indicates a gating mechanism, but further three properties of this motion have to be examined: occurrence of the open state, if the motion found with PLS is included in the main motion and if the channel is open simultaneously.
As the projection value of the PLS vectors describes the closed (negative) and open (positive) state of the channel, it will be called openness value and denoted as ξ_o.

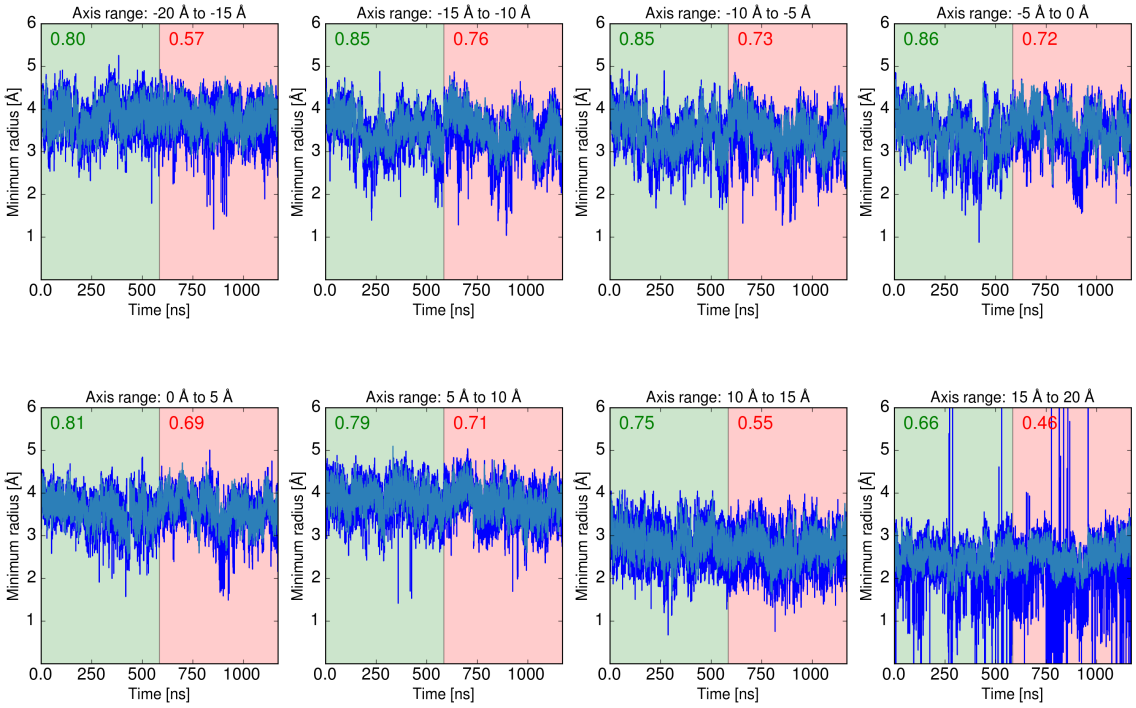

Figure 4.4.: Plots of the PLS FMA for the 8 different sections. The dark blue line is the minimal radius measured with HOLE, while the light blue line in the first half of the time (green background) represents the model and in the second half (red background) the cross-validation.

Occurrence of the open state

To see if the channel is mostly open or closed, a histogram with the openness value can be inspected. In figure 4.7 it can be seen that the channel is mostly closed. As no exact openness value can be assigned to an open or closed state, it is not possible to say what percentage of time the channel spends in a open state.

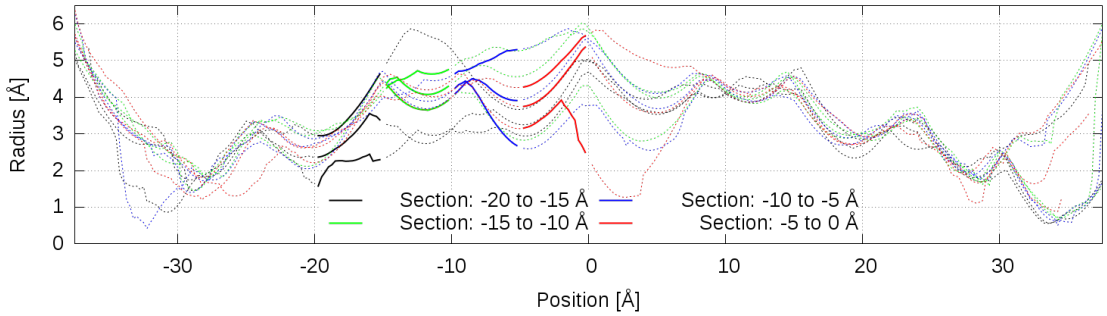

Figure 4.5.: Radius profiles of four different PLS vectors. From every plotted section the smallest, middle and biggest radius for the given section is plotted. In the region for which the PLS vector was trained the line is continuous, elsewhere doted. It can be seen that the four profiles are similar in the region $-20\,\text{Å} < z < 10\,\text{Å}$, while they differ in the trained region.

PLS vector compared to the PLC EV

For estimating if the main motions of the channel contain the PLS vector, the overlap (inner product) of the major PCA eigenvectors and the PLS vectors were calculated. As the PLS and PCA vectors are normalized before the multiplication the value of the scalar products depends only on the relative orentation of the PLS vecotrs to the EVs. The PCA analysis generates $1980 \cdot 3 = 5940$ eigenvectors, but already the first 10 EVs contribute to 99.3 % of the sum of all eigenvalues, while the first EV contributes 92.7 % to the sum of all eigenvalues. This means that the first ten EV are responsible for 92.7 % of the total fluctuation of the protein. Thus, only the scalar products of the PLS vectors with the first ten EVs will be analysed.

To determine the significance of resulting scalar products, the probability to get an inner product of two random vectors which is bigger than a given value will be calculated. The probability that the inner product of two normalized random vectors from a gaussian distribution in n-dimensional space is bigger than the value ε can be calculated using the regularized incomplete beta function by $I_{1-\varepsilon^2}(\frac{n-1}{2}, \frac{1}{2})$ (see appendix A for derivation). As most of the atoms are constrained by bonds to other atoms, using the total number of dimensions $n = 5940$ would not lead to a correct result. The artificial assumption that at least one atom of each of the approx. 270 residue can move freely in one direction leads to $n = 270$. In the following calculation this assumptions will be lowered to $n = 100$. Using the above formula with $n = 100$, it is possible to calculate the minimum inner product that has a 2σ and 3σ significance. The calculation yields that the minimal scalar product should be

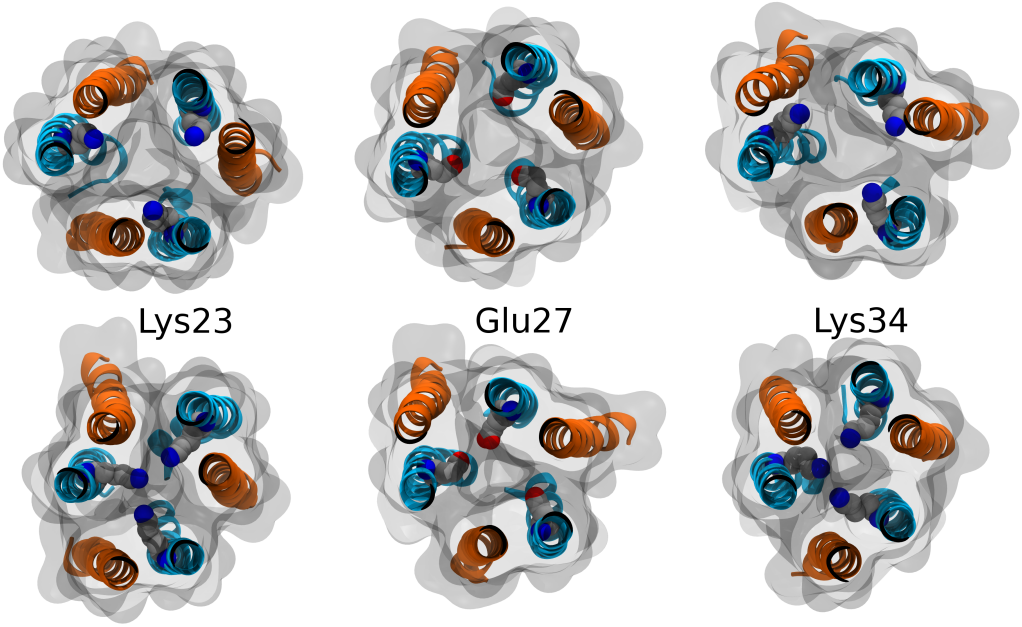

Figure 4.6.: The maximal open (top) and close (bottom) states of WT. For the three different pictures vectors from different sections were used (Lys23: −5 to 0 Å, Glu27: −10 to − 5 Å and Lys34: −20 to − 15 Å). The different colors of the backbones symbolize antiparallel orientation of the backbones and the gray area indicates the steric dimension of the channel.

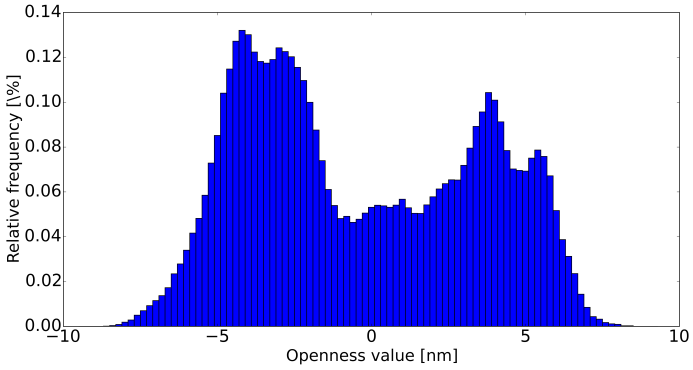

Figure 4.7.: The averaged openness value of the PLS vectors. The histogram contains the openness value of all PLS vectors from the simulation of WT used for PLS FMA. A negative value corresponds to an closed channel and positive value to a open one.

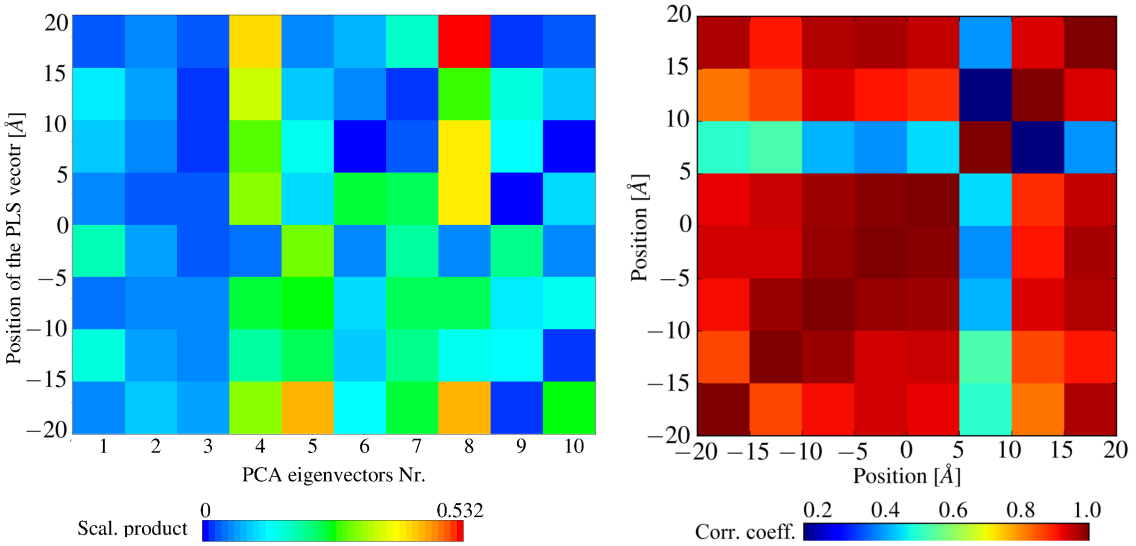

Figure 4.8.: (A) Matrix with scalar products of the ten PCA EVs with the highest eigenvalues and the PLS vectors. (B) Correlation matrix of the openness values $\xi_o(t)$ of different sections. The high correlations mean that nearly the whole channel is being opened simultaneously. Only one of the PLS vectors, from the section 5 to 10 Å , is not correlated with others.

higher than 0.198 for 2σ significance (green in figure 4.8 A) and higher than 0.291 for 3σ (yellow green in figure 4.8 A).

The first EV contributes 92.7 % to the sum of all eigenvalues and does not show a significant scalar product with the PLS vectors. Only the fourth EV, which contributes only 0.2 % to the sum of all eigenvalues, yields a significant scalar product with the PLS vectors. Thus it could only be shown here that the PLS motion is at least slightly included in the PCA EVs. As the PLS vectors could be compound of different PCA EV the particular scalar products would be called insignificant here. It is possible that PLS vectors are also partially included in the first three PCA EVs. The assumption of $n = 100$ is a lower limit, thus using a higher dimensional space could lead to the statement that also the scalar products of the FMA vectors with the first EV have a significant overlap. For example assuming $n = 800$, one could state a 3 σ significance of the scalar products between the PLC vectors and the first PVA EV. Although the calculation above used a comparatively small number of dimensions, no proof for the correctness of this lower limit can be provided.

Simultaneously opening of the channel

To see if the whole channel is open at the same time, the correlation between the

Mutant	ξ_o [nm]	σ_{ξ_o} [nm]	ξ_o [nm]	$\sigma_{\xi_o.}$ [nm]	
WT	-1.3537	1.75341	K23QE27Q	-1.23864	1.58156
WT_{DP}	-1.27045	1.78657	K23QK34Q	-1.55272	1.68096
E27Q	-1.41907	1.87557	$K23QK34Q_{DP}$	-1.81184	2.06712
K23DabE27D	-1.28143	1.31591	K23SK34S	-1.42002	1.89348
K23HE27D	-1.19499	1.92196	K23QE27QK34Q	-1.19759	1.40156

Table 4.1.: The openness value averaged over all sections of all simulations and channels of a given mutant.

eight openness values from the different sections can be calculated (see figure 4.8 B). A correlation coefficient of one would mean that the whole channel is opening at the same time, while minus one would mean that one part is closing while another part is opening. As most of the correlation coefficients are higher than 0.7, it can be assumed that the opening of the different section of the channel is mostly correlated and in any case not anticorrelated.

4.3.2. Open/closed state in the CEP simulations

The openness value from the eight sections of the simulation runs of the mutants are shown in table 4.1. As the projection of a vector can only be calculated on the same structure as the one that was used for calculating the vector, the residues on the positions 23, 27 and 34 were excluded from the calculation. Instead, only the first three carbon atoms of these residues were used for the calculations.
All mutants are close to the closed state but show a relatively large standard deviation. In contrast to the simulations without TMV, the distribution of the openness values can be approximated by a single gaussian function and not by two gaussian functions (data not shown).
As long as a bacteria is alive it possesses a transmembrane potential. If the opening mechanism that is investigate here would be an voltage gating, one would expect a positive average openness value of about $\xi_o \approx 5$nm like in the right peak in figure 4.7. This result can be interpreted as an indication that the opening mechanism of DCD-1L is not a voltage gating.

4.3.3. Essential dynamics

For performing the ED simulation the PLS FMA vector from the section between $z = -20\,\text{Å}$ and $z = -15\,\text{Å}$ was used. The simulations were performed at six different openness values $\xi_o = (-5, -3, -1, 1, 3, 5)\,\text{nm}$. The expected profiles which were obtained from the PLS vectors and the resulting ones which are the results of the averaging of all channels of a given openness value can be seen in figure 4.10. While the profiles in the section where the radius should change show a smaller change than expected but still a significant one, the radius in the region 25 to 35Å acts contradictorily to the PLS vector and closing the right end opening.
At the end of the channel there is an increasing conductance when the openness value is increased (see figure 4.9). Only the data point at $\xi_o = -5\,\text{nm}$ does not fit in this upward trend. Using all six data points yields a correlation coefficient of $R_C = 0.629$ and $p_{R_C=0.63} = 0.181$, while using all but the first data point yields $R_C = 0.976$ and $p_{R_C=0.976} = 0.004$.
Using a linear regression to estimate the relation between the openness value and the conductance $G(\xi_o) = m \cdot \xi_o + a$ yields the parameters $m = (4.6 \pm 1.8)\text{pS/nm}$ and $a = (32.7 \pm 4.6)\text{pS}$. Inserting the average projection value for WT from the table 4.1 results in the conductance $G(1.4\,\text{nm}) = (33 \pm 10)\,\text{pS}$, what is in full agreement with the value of $G_{WT} = (34 \pm 5)\text{pS}$ Although the radius profiles do not show as large differences as predicted, the ED simulations produce the expected result that the conductance dependences on the openness value and is in agreement with the conductance value of WT in figure 4.11.
Despite these results, there are still some issues that can not be explained. The fact that the channel does not have the planned radius profiles but exhibits the adjusted openness value, could mean that the PLS values vectors are not the optimal choice for the ED simulation. In addition the PLS vector was trained only on one section of the channel, but as mentioned earlier the channel opens simultaneously and thus a vector that describes the opening mechanism of the whole channel would probably produce more accurate results. It is possible that the channel can not be open only partially like it is being attempted here.

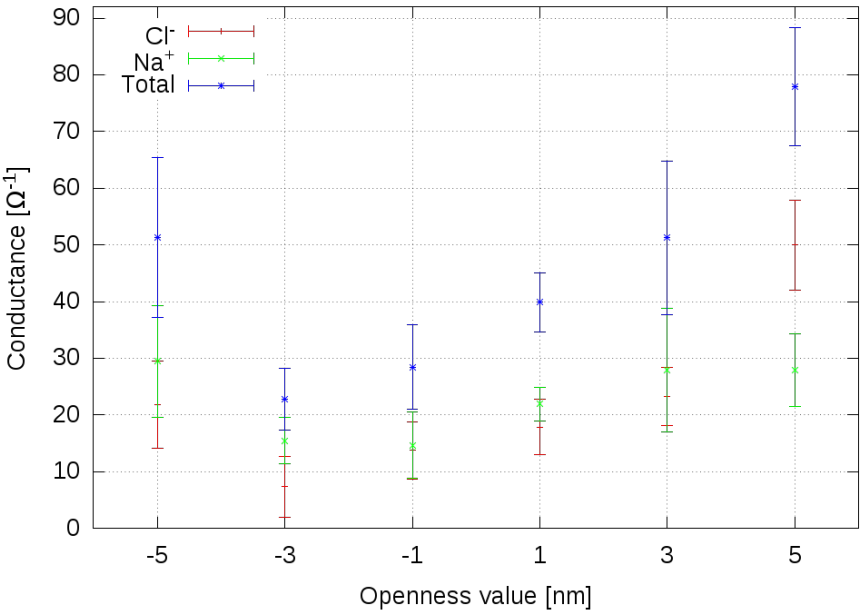

Figure 4.9.: Conductance of the ED simulations of WT plotted against openness value. For the ED simulation the PLS vector from section -15 to -10 Å was used.

4.4. Properties of the mutants as an AMP

The dermcidins known mechanism of killing bacteria can be divided in two parts: the binding to the membrane, which also involves the oligomerization and penetrating of the membrane, and the acting as an ion channel. As the mean hydrophobicity and the mean amphipatic moment are responsible for the interaction if the AMP with the membrane, it has to be guaranteed that they are not reduced.
In the case of K23SK34S the mean hydrophobicity was increased by 19 % while the hydrophobic moment was decreased by 5 %. Due to the risen negative net charge, it is not possible to say if K23SK34S will exhibit the same affinity to negative membranes.
The possibility of raising H and $\langle \mu_H \rangle$ without influencing the conductance was tested on K23QE27QK34Q by mutations concerning only residues outside of the channel. The result can be summarised that it is possible but not always true. While QQQLLL show a by $\Delta G = (41 \pm 9)$ pS reduced conductance and also a reduced radius profile, posses QQQVLLL nearly the same conductance as K23QE27QK34Q as it differs by only $\Delta G = (12 \pm 10)$ pS.
QQQVLL has a only slightly higher negative net charge by having at the same time a by 62 % increased mean hydrophobicity and by 9 % increased amphipathic

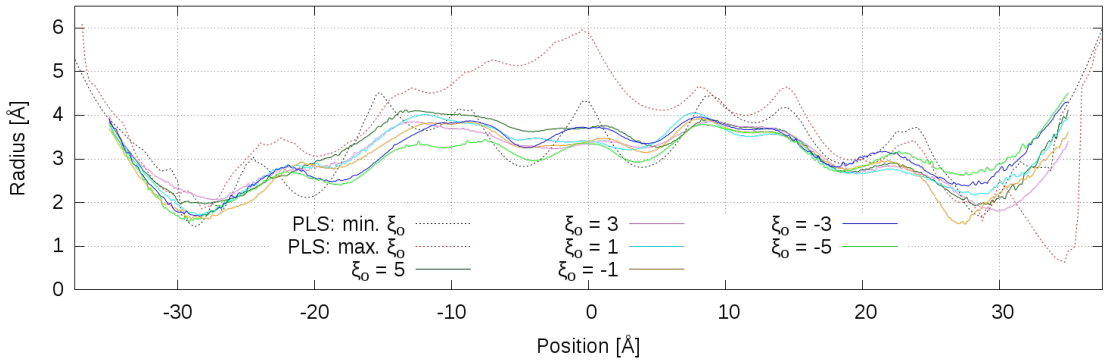

Figure 4.10.: Radius profiles of two PLS vectors (dotted lines) and of the channels from the ED simulations. The two dotted lines are the minimum and maximum profiles from PLS FMA that were expected in the ED simulations. The continuous lines represent the radius profiles that were obtained by averaging the profile over all ED simulations of a given openness value. The dark green line represent the most open and the light green the most closed channel.

Mutant	Q [e]	$\langle H \rangle$	$\langle \mu_H \rangle$	Polar residues [%]	Instability index
DCD	-3	0.206	0.453	60.42	10.13
K23SK34S	-4 1/3	0.245	0.430	60.42	15.43
QQQ	-3 1/3	0.247	0.427	60.42	19.44
QQQLLL	-3 1/3	0.334	0.495	60.42	19.44
QQQVLLL	-3 1/6	0.375	0.490	58.33	13.86

Table 4.2.: Table with properties of mutants that influence their antimicrobial activity: net charge Q in the alternative protonation state, Mean hydrophobicity $\langle H \rangle$, Mean amphipathic moment $\langle \mu_H \rangle$, content of polar residues and the instability index, which ranges from 0 to 100.

moment. Thus it is possible that this mutant will have a high haemolytic activity and can not be used medically.

The instability of all mutants is slightly increased, but no value exceeds 40, which means that all mutants should be stable. Another result would be surprising, as all mutants were stable in the simulations. As the instability index was only made to predict if a protein is stable or not and not to compare the stability of stable proteins no further statements are possible.

4.5. Conductance

4.5.1. Dermcidin and Protonation State

The conductance of the WT with different protonation states differs by $\Delta G_{WT} = (82 \pm 14)\,\mathrm{pS}$ and can not be explained by statistical error. Thus it means that the conductance of the channel depends on the protonation state of the peptide. Because of the uncertainty of the true protonation state, a comparison with other values can help to estimate the correctness of the results:

- $G_1 = (108 \pm 11)\,\mathrm{pS}$ (Simulation, 1 M NaCl at ca. 0.2 V [61])
- $G_2 = (62 \pm 8)\,\mathrm{pS}$ (Simulation, 0.15 M NaCl at ca. 0.5 V [22])
- $G_3 = (81 \pm 14)\,\mathrm{pS}$ (Experimental, pH 7.1 and 1 M NaCl at 100 mV [61])
- $G_4 \approx 30\,\mathrm{pS}$ (Experimental, pH 6.0 and 1 M KCl at 100 mV; higher conductance up to 150 pS were measured at $10mV$ mV[52])

As the simulation of $\mathrm{WT_{DP}}$ is practically the same as performed in [61], also the values of conductance are nearly the same. In the simulation in [22] a lower molarity was used, so that also the conductance is smaller. Unfortunately the conductance G_4 was obtained using potassium which has a 20 % greater van der Waals radius than sodium. Thus it is not possible to determine if G_4 is smaller than G_3 due to the lower pH value. At the end it is not possible to say if the discrepancy of the conductance in the performed simulations is a real feature of dermcidin or an effect of a wrong protonation state.
The default protonation of K23QK34Q show a $\Delta G_{K23QK34Q} = (34.86 \pm 22.47)\,\mathrm{pS}$ higher value of conductance. The fact that two default protonation states have a higher conductance than the alternative one, indicates that this also could be true for the other mutant. Due the small amount of samples this statement can not be considered as statistically firm.

4.5.2. Dependence on radius profile and charged residues

As all mutants were simulated in the alternative protonation state, the conductance of WT and not of $\mathrm{WT_{DP}}$ will be used as a reference value.
Looking at only one property, like radius profile or net charge, no correlation to

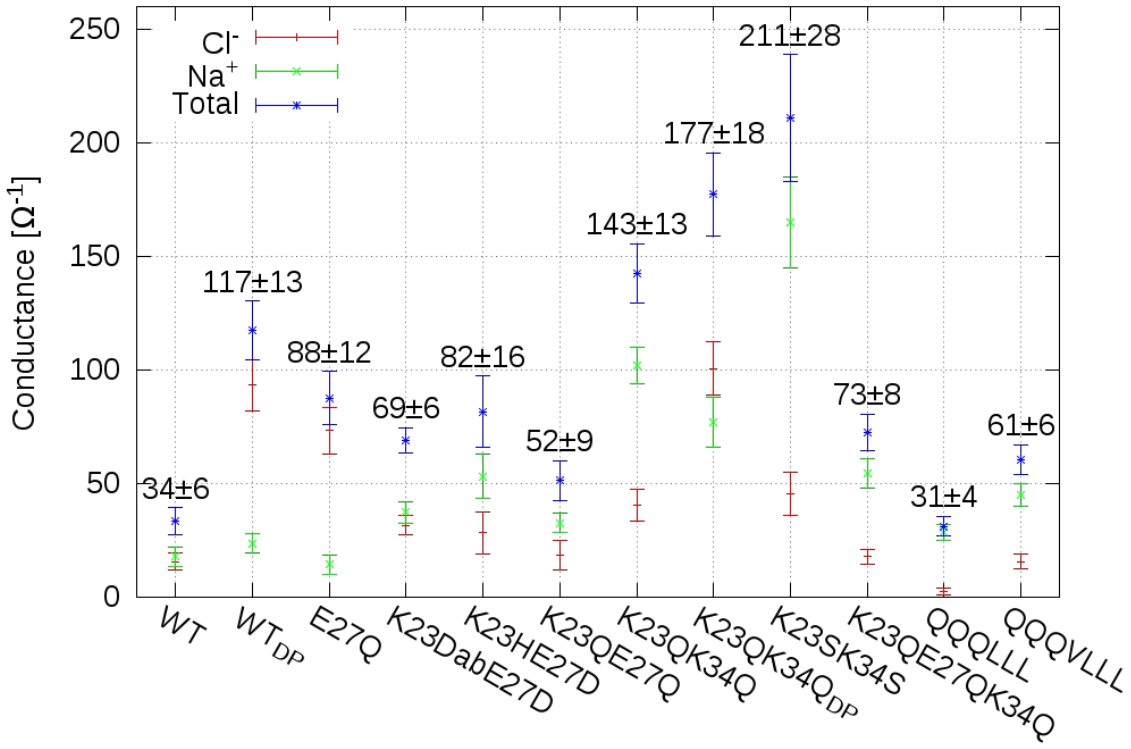

Figure 4.11.: Conductances of all simulated mutants averaged over all simulations of a given mutant.

an increased conductance can be found. While the two mutants with the highest conductance have a changed net charge by -8 e, the next three best mutants, which have overlapping errorbars, show a changed net charge relative to WT by -2 e, 0 e, and + 6 e.

No correlation between high conductance and high radius could be found. For example K23QK34Q and K23QE27QK34Q have a nearly the same radius profile, but K23QK34Q possesses a twice as high conductance than the conductance of K23QK34Q. Another example is E27Q which has the smallest radius on average and one of the highest conductances.

The two highest conductances are achieved by K23QK34Q and K23SK34S. K23QK34Q possesses a similar radius profile like WT_{DP} and thus the high conductance can not be explained by the radius profile. In contrast K23SK34S exibits the biggest average radius and the highest conductance of all tested mutants. These results imply that the conductance primarily depends on the position of mutation and secondarily on the length of the inserted residue. Also the mutants K23HE27D and K23DabE27D

exhibit a higher conductance and increased radius compared to K23QE27Q. The fact that glutamine is, in in contrast to the charged protonated histidine, aspartic acid and diaminobutyric acid, neutral does not seem to play a role.
At the end mutating the residues K23 and E34 to the short polar amino acid serine produces the best result. Serine is in fact the shortest amino acid that can be used for the mutation here, as glycine, the only one natural hydrophilic amino acid shorter than serine, tends to destabilize α-helices [44].

5. Discussion

5.1. Prototonation state

As WT_{DP} possesses a radius profile which does not differ between different simulation runs as much as WT, this could mean that WT_{DP} has a more stable structure. Although ions use the openings at the channel termini more often in the simulations of WT than in this of WT_{DP}, the dermcidin channel shows a higher conductance in default protonation. These results suggest that the default protonation is the protonation state that can be found in nature. Since this study focused on the alternative state, it is left for future research to determinate the true protonation state of dermcidin.
As the alternative protonation state is calculated for a pH value of 5 and the default protonation uses the protonation state of amino acids at a pH value of 7, it is possible that both investigated protonations are true at different pH values. The easiest way to test the dependence of DCD-1L on the pH value would be an experiment.
Since the protonation state of dermcidin has a large influence on the conductance, it could be crucial for further investigations to determine it.

5.2. Improving antimicrobial activity of dermcidin by mutations

Radius profiles and conductance

The initial motivation of this study was to raise the conductance of dermcidin by increasing the radius of the channel. For this the residues that most extend into the interior of the channel were identified. It seems that the radius profile, that results from mutation of these residues, has a secondarily importance. Instead the conductance of the channel appear to dependent primarily on the position where the mutation was performed. This result together with the motion of these residues

which was found using PLS FMA imply that the residues K23, E27 and K34 could be of particular importance for dermcidin.

Interaction of the mutants with bacteria membrane

The mutations that increase the conduction of the channel can lead to a lowered affinity of the peptide for membranes. In this case further mutation to contract this problem are needed. The two mutants of K23QE27QK34Q show that it is possible to raise $\langle H \rangle$ and $\langle \mu_H \rangle$ without affecting G significantly. A crucial property for future research is the haemolytic activity. It could be that it is not possible to raise the interaction between the mutant and a bacteria membrane without raising the haemolytic activity too much. Although computational predictions of haemolytic activity are possible, only experiments can produce reliable data [15].

Function of the residues K23, E27 and K34

All mutations investigated here concern the three residues K23, E27 and K34, which limit the channel radius of DCD-1L. But no reason is known why these long residues are inside the channel. One possibility would be, that these three residues are needed for penetration of the membrane because long hydrophobic amino acids allow a deeper insertion into the bilayer [68]. Thus it is possible that the observed closing/opening mechanism is a necessary compromise: K23, E27 and K34 must be there for the insertion into the membrane but disturb the ion flow afterwards. To resolve this question, further simulations that concern the interaction of mutants with the membrane and penetration of the membrane are needed.

Influence of the openness value on the conductance

Investigations on a possible gating mechanism of dermcidin reveals that the radius can increase in particular place by more than 2 nm, this can be seen in figure 4.5. It was not possible to make a clear statement about how far this opening/closing mechanism is contained in the fluctuation of the channel. Instead the performed ED simulations show that it can affect the conductance positively. This could be used to make additional mutations which stabilise the mutant in an open state.

Most promising mutant

As the mutant K23SK34S possesses a six times higher conductance than WT and twice higher than $\mathrm{WT_{DP}}$, it is a promising candidate for AMP with a higher antimicrobial activity. Only increasing the conductance would not yield a better AMP, as

the interaction of the mutant with the bacteria membrane has to be preserved. As it can be seen in table 4.2, K23SK34S has a higher negative charge, an increased mean hydrophobicity and lowered amphipathic moment, so that it is not possible to make any clear prediction about the antimicrobial effect of K23SK34S. At the current state of research only further experiments could answer this question.

Educated guess for a further mutation

Although no mutant that has increased G, $\langle H \rangle$ and $\langle \mu_H \rangle$ was made, probably no much effort has to be made for such a mutant. A promising candidate is the combination of K23SK34S and QQQVLLL, which would result in SSVLLL (K23SK34S and A11LA14LD28VA34L). However, the mutant QQQLLL demonstrate that an educated guess could also be wrong. Although QQQLLL differs from QQQVLLL in one mutated residue which is outside the channel interior, QQQLLL has only the half of the conductance of QQQVLLL.

The mode of action of AMPs is sufficiently discovered, so that one can mutate AMPs on the basis of educated guesses. In addition various templates (like [68]) and prediction tools (for example [65]) that can help to estimate properties of AMPs are available. At the end investigating the properties by MD simulations and the mentioned aids can lead to promising candidates that could have a high minimal inhibitory concentration (MIC).

The development or discovery of an antibiotic with a high MIC and low haemolytic activity is the first step to production of an antimicrobial drug.

5.3. An example for medical use

Although the first AMP was discovered in 1939 [53], no references in literature about AMPs in medical use could be found. The first time that an AMP was tested in phase III of a clinical trial was in 1997 [45]. The tested drug was an antimicrobial topical cream with pexiganan as the active ingredient, but it is not approved in the U.S. until now. Pexiganan is an analogue of magainin AMPs, a class of antimicrobial peptides found on the skin of an African frog. Although the clinical benefits of pexiganan could be proved, it was not approved by the Food and Drug Administration (FDA) because of difficulties with manufacturing of the drug. After pexiganan was modified to meet the requirements of the FDA, currently a new phase III study is taking place.

As dermcidin is also an AMP that act on skin, it is plausible that it could also be also used as an antimicrobial topical cream. As no evidence about an intravenous or oral application of AMP based drug were found in literature, it is unlikely that dermcidin or any other AMP could be used to replace common antibiotics in the near future. The fact that nature created these AMPs to act on skin underlines this statement.

A. Appendix

Protonation state used in simulations

amino acid	chain	pos.	state	amino acid	chain	pos.	state
LYS	A	12	deprot.	ASP	C	45	prot.
LYS	A	34	deprot.	LYS	F	12	deprot.
LYS	A	41	deprot.	LYS	F	34	deprot.
ASP	A	45	prot.	LYS	F	41	deprot.
LYS	B	12	deprot.	ASP	F	45	prot.
ASP	B	28	prot.	LYS	G	12	deprot.
LYS	B	34	deprot.	ASP	G	28	prot.
ASP	B	45	prot.	LYS	G	34	deprot.
LYS	C	12	deprot.	ASP	G	45	prot.
LYS	C	20	deprot.	LYS	H	12	deprot.
ASP	C	28	prot.	ASP	H	28	prot.
LYS	C	34	deprot.	LYS	H	34	deprot.
LYS	C	41	deprot.	LYS	H	41	deprot.
ASP	H	45	prot.				

Table A.1.: The alternative protonation state that was used in most of the simulation uns was calculated by Chen Song

Derivation of the calculation of probability for getting a higher inner product of two random vectors than a given value

The probability that the product of two normalized random vectors $\mathbf{v}, \mathbf{w} \in \mathbb{R}^n$ from a gaussian distribution has a bigger value than ε, can be interpreted as the ratio of the area $S_{1-\varepsilon,n}$ of the hyperspherical cap with height $1-\varepsilon$ to the total area of the unit hypersphere S_n (see figure A.1). Because here the probability of the absolute value of the inner product is calculated, the area of $S_{1-\varepsilon,n}$ has to be multiplicated by two: $P(|\mathbf{v} \cdot \mathbf{w}| \geq \varepsilon) = 2S_{1-\varepsilon,n}/S_n$. Using the formulas for the area of a hyperspherical cap $S_{h,n} = \frac{1}{2} S_n r^{n-1} I_{(2rh-h^2)/r^2}(\frac{n-1}{2}, \frac{1}{2})$ [42], where $I_z(a,b)$ is the regularized incomplete beta function. Inserting the radius $r = 1$ and the height $h = 1 - \varepsilon$ leads to:

$$\frac{2S_{1-\varepsilon,n}}{S_n} = 2\frac{\frac{1}{2}S_n I_{(2(1-\varepsilon)-(1-\varepsilon)^2)}(\frac{n-1}{2}, \frac{1}{2})}{S_n} = I_{1-\varepsilon^2}(\frac{n-1}{2}, \frac{1}{2}) \ .$$

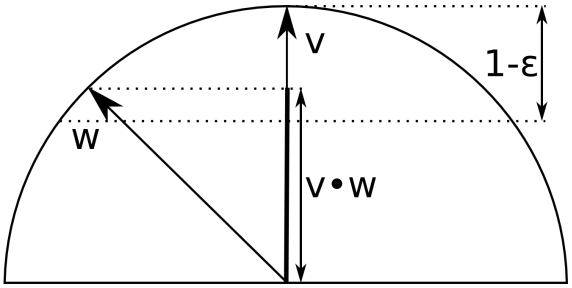

Figure A.1.: Two dimensional geometrical explanation of the calculation of the relation $P(|\mathbf{v} \cdot \mathbf{w}| \geq \varepsilon) = 2S_\varepsilon/S_n$, where $\mathbf{v}, \mathbf{w}$ are normalized vectors. The vector $\mathbf{v}$ is aligned to the y-axis, while $\mathbf{w}$ has still a random position. If the inner product of the vectors $\mathbf{v}, \mathbf{w}$ should be bigger than ε, then the vector $\mathbf{w}$ has to point to the area of the spherical cup with the hight $1 - \varepsilon$. The probability that this will happen is proportional to the area of the spherical cup.

Bibliography

[1] Avanti Polar Lipids - Discover the Difference... www.avantilipids.com/, Accessed: 09.09.2014. Note: The formulas of the lipid tails were found using the search function on the main page.

[2] gmx make_edi. http://manual.gromacs.org/programs/gmx-make_edi.html, Accessed: 14.09.2014.

[3] B. Alberts, A. Johnson, J. Lewis, M. Raff, K. Roberts, and P. Walter. *Molecular biology of the cell*. Garland Science, 2002.

[4] A. Amadei, A. B. M. Linssen, B. L. de Groot, D. M. F. van Aalten, and H. J. C. Berendsen. An efficient method for sampling the essential subspace of proteins. *J. Biomol. Struct. Dyn.*, 13:615–626, 1996.

[5] A. A. Bahar and D. Ren. Antimicrobial peptides. *Pharm. J.*, 6:1543–1575, 2013.

[6] D. Bashford and K. Gerwert. Electrostatic calculations of the pKa values of ionizable groups in bacteriorhodopsin. *J. Mol. Biol.*, 11:6, 1992.

[7] L. Becucci, D. Valensin, M. Innocenti, and R. Guidelli. Dermcidin, an anionic antimicrobial peptide: influence of lipid charge, pH and Zn2+ on its interaction with a biomimetic membrane. *Soft Matter*, 10:616–626, 2014.

[8] H. J. C. Berendsen, J. P. M. Postma, W.F. Van Gunsteren, A. DiNola, and J. R. Haak. Molecular dynamics with coupling to an external bath. *J. Chem. Phys.*, 81:3684–3690, 1984.

[9] R. A. Bonham, L. S. Bartell, and D. A. Kohl. The molecular structures of n-pentane, n-hexane and n-heptane. *J. Am. Chem. Soc.*, 81:4765–4769, 1959.

[10] O. Braun-Falco, G. Plewig, H. H. Wolff, W. H. C. Burgdorf, and M. Landthaler. *Dermatologie und Venerologie*. Springer Medizin Verlag Heidelberg, 2005.

[11] K. A. Brogden. Antimicrobial peptides: pore formers or metabolic inhibitors in bacteria? *Nat. Rev. Microbiol.*, 3:238–250, 2005.

[12] M. J. Buono, K. D. Ball, and F. W. Kolkhorst. Sodium ion concentration vs. sweat rate relationship in humans. *J. Appl. Physiol.*, 103:990–994, 2007.

[13] G. Bussi, D. Donadio, and M. Parrinello. Canonical sampling through velocity rescaling. *J. Chem. Phys.*, 126:014101, 2007.

[14] C. N. Connolly and K. A. Wafford. The cys-loop superfamily of ligand-gated ion channels: the impact of receptor structure on function. *Biochem. Soc. Trans.*, 32:529–534, 2004.

[15] M. Dathea, T. Wieprechta, H. Nikolenkoa, L. Handela, W. L. Maloyb, D. L. MacDonaldb, M. Beyermanna, and M. Bienerta. Hydrophobicity, hydrophobic moment and angle subtended by charged residues modulate antibacterial and haemolytic activity of amphipathic helical peptides. *FEBS Lett.*, 403:208–212, 1997.

[16] M. C. Denham. Implementing partial least squares. *Stat. Comput*, 5:191–202, 1995.

[17] Erick J. Dufourc. Sterols and membrane dynamics. *J. Chem. Biol.*, 1:63–77, 2008.

[18] B. Efron. Bootstrap methods: Another look at the jackknife. *Ann. Stat.*, 7: 1–26, 1979.

[19] D. Eisenberg, R. M. Weiss, and T. C. Terwilliger. The helical hydrophobic moment: a measure of the amphiphilicity of a helix. *Nature*, 299:371–374, 1982.

[20] U. Essmann, L. Perera, M. L. Berkowitz, T. Darden, H. Lee, and L. G. Pedersen. A smooth particle mesh ewald method. *J. Chem. Phys.*, 103:8577–8593, 1995.

[21] J. Fauchere and V. Pliska. Hydrophobic parameters pi of amino-acid side chains from the partitioning of n-acetyl-amino-acid amides. *Eur. J. Med. Chem.*, 8: 369–375, 1983.

[22] B. Forsberg. The antimicrobial effect of dermcidin investigated by computational electrophysiology molecular dynamics simulations. Master's thesis, Department of Biochemistry and Biophysics, Stockholm University, 2013.

[23] R. Gautier, D. Douguet, B. Antonny, and G. Drin. HELIQUEST: a web server to screen sequences with specific alpha-helical properties. *Bioinformatics*, 24: 2101–2102, 2008.

[24] D. Gfeller, O. Michielin, and V. Zoete. SwissSidechain: a molecular and structural database of non-natural sidechains. *Nucleic Acids Research*, 41:D327–D332, 2013.

[25] K. Guruprasad, B.V.B. Reddy, and M.W. Pandit. Correlation between stability of a protein and its dipeptide composition: a novel approach for predicting in vivo stability of a protein from its primary sequence. *Protein Eng.*, 4:155–161, 1990.

[26] B. Hess, H. Bekker, H. J. C. Berendsen, and J. G. E. M. Fraaije. LINCS: A linear constraint solver for molecular simulations. *J. Comput. Chem.*, 18: 1463–1472, 1997.

[27] B. Hess, C. Kutzner, D. van der Spoel, and E. Lindahl. GROMACS 4: Algorithms for highly efficient, load-balanced, and scalable molecular simulation. *J. Chem. Theory Comp.*, 4:435–447, 2008.

[28] B. Hille. *Ion Channels of Excitable Membranes*. Sinauer Associates, Inc., 2001.

[29] Wu Hongyu. Lamp database. `http://biotechlab.fudan.edu.cn/database/lamp/detail.php?id=L01A000260`, Accessed: 08.06.2014.

[30] J. S. Hub and B. L. de Groot. Detection of functional modes in protein dynamics. *PLoS Comput. Biol.*, 5:e1000480, 2009.

[31] J. S. Hub, B. L. de Groot H. Grubmüller, and G. Groenhof. Quantifying artifacts in ewald simulations of inhomogeneous systems with a net charge. *J. Chem. Theory Comput.*, 10:381–390, 2014.

[32] W.B. Hugo and A.D. Russell. *Hugo and Russell's pharmaceutical microbiology*. Blackwell Publishing, 2004.

[33] S. Jo, T. Kim, V. G. Iyer, and W. Im. CHARMM-GUI: A web-based graphical user interface for CHARMM. *J. Comput. Chem.*, 29:185–1865, 2008.

[34] H. H. Jung, S. T. Yang, J. Y. Sim, S. Lee, J. Y. Lee, H. H. Kim, S. Y. Shin, and J. I. Kim. Analysis of the solution structure of the human antibiotic peptide dermcidin and its interaction with phospholipid vesicles. *BMB Rep.*, 43:362–368, 2010.

[35] Berk Hess K. Anton Feenstra and Herman J. C. Berendsen. Improving efficiency of large time-scale molecular dynamics simulations of hydrogen-rich systems. *J. Comp. Chem.*, 20:786–798, 1999.

[36] J.B. Klauda, R.M. Venable, J.A. Freites, J.W. O'Connor, D.J. Tobias, C. Mondragon-Ramirez, I. Vorobyov, Jr. A.D. MacKerell, and R.W. Pastor. Update of the CHARMM all-atom additive force field for lipids: Validation on six lipid types. *J. Phys. Chem. B*, 114:7830–7843, 2010.

[37] T. Krivobokova, R. Briones, J. S. Hub, A. Mun, and B. L. de Groot. Partial least-squares functional mode analysis: Application to the membrane proteins AQP1, Aqy1, and CLC-ec1. *Biophys. J.*, 103:786–796, 2012.

[38] C. Kutzner, H. Grubmüller, B. L. de Groot, and U. Zachariae. Computational electrophysiology: The molecular dynamics of ion channel permeation and selectivity in atomistic detail. *Biophys. J.*, 101:809–817, 2011.

[39] C. Kutzner, H. Grubmüller, B. L. de Groot, and U. Zachariae. Simulation Setup of Computational Electrophysiology. `www.mpibpc.mpg.de/13829367/Fig01-SimulationSetup.pdf`, 2011. Accesed: 10.09.2014.

[40] Y. Lai, A. E. Villaruz, M. Li, D. J. Cha, D. E. Sturdevant, and M. Otto. The human anionic antimicrobial peptide dermcidin induces proteolytic defence mechanisms in staphylococci. *Mol. Microbiol.*, 63:497–506, 2007.

[41] G. Laverty, S. Gorman, and B. Gilmore. The potential of antimicrobial peptides as biocides. *Int. J. Mol. Sci.*, 12:6566–6596, 2011.

[42] S. Li. Concise formulas for the area and volume of a hyperspherical cap. *Asian J. Math. Stat.*, 4:66–70, 2011.

[43] S. B. Long, X. Tao, E. B. Campbell, and R. MacKinnon. Atomic structure of a voltage-dependent K+ channel in a lipid membrane-like environment. *Nature*, 450:376–382, 2007.

[44] J. Lopez-Llano, L. A. Campos, and J. Sancho. Alpha-helix stabilization by alanine relative to glycine: roles of polar and apolar solvent exposures and of backbone entropy. *Proteins*, 64:769–778, 2006.

[45] D. P. Luci and D. Garrett. Dipexium pharmaceuticals initiates pivotal phase 3 clinical trial of locilex in patients with mild infections of diabetic foot ulcers. `http://content.stockpr.com/_news/dipexiumpharmaceuticals/2014-07-17_Dipexium_Pharmaceuticals_Initiates_Pivotal_Phase_3_54.pdf`, Accessed: 08.09.2014.

[46] E. Matyus, C. Kandt, and D. P. Tieleman. Computer simulation of antimicrobial peptides. *Curr. Med. Chemistry*, 14:2789–2798, 2007.

[47] S. J. Montain, S. N. Cheuvront, and Henry C. Lukaski. Sweat mineral-element responses during 7 h of exercise-heat stress. *Int. J. Sport Nutr. Exerc. Metab.*, 17:574–582, 2007.

[48] S. Morein, A. Andersson, L. Rilfors, and G. Lindblom. Wild-type escherichia coli cells regulate the membrane lipid composition in a window between gel and non-lamellar structures. *J. Biol. Chem.*, 271:6801–6809, 1996.

[49] J. Niskanen and H. Henschel. Molecular Dynamics Simulations. `www.courses.physics.helsinki.fi/fys/moldyn/lectures/L2.pdf`, Autumn 2013. Accesed: 10.09.2014.

[50] R. Notmana and J. Anwarb. Breaching the skin barrier - insights from molecular simulation of model membranes. *Adv. Drug Deliv. Rev.*, 65:237–250, 2013.

[51] S. Pall and B. Hess. A flexible algorithm for calculating pair interactions on SIMD architectures. *Adv. Drug Deliv. Rev.*, 184:2641–2650, 2013.

[52] M. Paulmann, T. Arnold, D. Linke, S. Ozdirekcan, A. Kopp, T. Gutsmann, H. Kalbacher, I. Wanke, V. J. Schuenemann, M. Habeck, J. Burck, A. S. Ulrich, and B. Schittek. Structure-activity analysis of the dermcidin-derived peptide DCD-1L, an anionic antimicrobial peptide present in human sweat. *J. Biol. Chem.*, 287:8434–8443, 2012.

[53] D. A. Phoenix, S. R. Dennison, and F. Harris. *Antimicrobial Peptides*. Wiley-VCH, 2013.

[54] JP. Powers and R. Hancock. The relationship between peptide structure and antibacterial activity. *Peptides*, 24:1681–1691, 2003.

[55] S. Rieg, H. Steffen, S. Seeber, A. Humeny, H. Kalbacher, K. Dietz, C. Garbe, and B. Schittek. Deficiency of dermcidin-derived antimicrobial peptides in sweat of patients with atopic dermatitis correlates with an impaired innate defense of human skin in vivo. *J. Immunol.*, 174:8003–8010, 2005.

[56] M. Rostkowski, M. H. M. Olsson, C. R. Søndergaard, and J. H. Jensen. Graphical analysis of pH-dependent properties of proteins predicted using propka. *BMC Struct. Biol.*, 11:473–486, 2011.

[57] P. Rostock. *Die Wunde*. de Gruyter, 1950.

[58] J. N. Sachs, P. S. Crozier, and T. B. Woolf. Atomistic simulations of biologically realistic transmembrane potential gradients. *J. Chem. Phys.*, 121:10847–10851, 2004.

[59] Schrödinger, LLC. The PyMOL molecular graphics system, version 1.7.0.5, 2010.

[60] O. S. Smart, J. G. Neduvelil, X. Wang, B. A. Wallace, and M. S. P. Sansom. HOLE: A program for the analysis of the pore dimensions of ion channel structural models. *J. Mol. Graphics*, 14:354–360, 1996.

[61] C. Song, C. Weichbrodt, E.S. Salnikov, M. Dynowski, B.O. Forsberg, B. Bechinger, C. Steinem, B.L. de Groot, U. Zachariae, and K. Zeth. Crystal structure and functional mechanism of a human antimicrobial membrane channel. *PNAS*, 110:4586–4591, 2013.

[62] M. Tarek. Membrane electroporation: A molecular dynamics simulation. *Biophys. J.*, 88:4045–4053, 2005.

[63] C. J. Thomson, E. Power, H. Ruebsamen-Waigmann, and H. Labischinski. Antibacterial research and development in the 21(st) century–an industry perspective of the challenges. *Curr. Opin. Microbiol.*, 7:445–50, 2004.

[64] D. van der Spoel, E. Lindahl, B. Hess, G. Groenhof, A. E. Mark, and H. J. C Berendsen. GROMACS: Fast, flexible and free. *J. Comp. Chem.*, 26:1701–1718, 2005.

[65] F. H. Waghu, L. Gopi, R. S. Barai, P. Ramteke abd B. Nizami, and S. Idicula-Thomas. CAMP: Collection of sequences and structures of antimicrobial peptides. *Nucleic Acids Res.*, 42:1154–1158, 2014.

[66] M. G. Wolf, M. Hoefling, C. Aponte-SantamarÃa, H. Grubmüller, and G. Groenhof. g_membed: Efficient insertion of a membrane protein into an equilibrated lipid bilayer with minimal perturbation. *J. Comput. Chem.*, 31: 2169–2174, 2010.

[67] M. R. Yeaman and N. Y. Yount. Mechanisms of antimicrobial peptide action and resistance. *Pharmacol. Rev.*, 55:27–55, 2003.

[68] I. Zelezetsky and A. Tossi. Alpha-helical antimicrobial peptides–using a sequence template to guide structure-activity relationship studies. *Biochim. Biophys. Acta*, 1758:1436–1449, 2006.

Acknowledgements

It is a great honor for me to acknowledge the help of Prof. Bert de Groot, who gave me the opportunity to join the computational biomolecular dynamics group and supported me during the whole period of my bachelor's thesis. He always had time to discuss problems of my bachelor's thesis and to assist me with his knowledge and experience. As he had time for all the questions I had and let me choose the topics I was interested in, I learned much about scientific and independent work.
Furthermore, it was a pleasure to be able to work in this group, which made my studies here highly enjoyable. All members were very friendly and helpful, whenever I walked into somebody's office seeking for help I got great support.
I am especially indebted to Rodolfo Briones and Shreyas Kaptan for their individual expertise in numerous discussions. Without them my bachelor's thesis would have stayed a dream.
This thesis would also not have been possible without the computational resources that Prof. Bert de Groot allowed me to use. Thus, I am also grateful to the Max Planck Society and Prof. Bert de Groot for his trust in me. The people who made it possible for me to use the cluster and were maintaining it are Ansgar Esztermann and Martin Fechner. I thank them for this and also for their support with all computer problems I had.

Erklärung nach §13(8) der Prüfungsordnung für den Bachelor-Studiengang Physik und den Master-Studiengang Physik an der Universität Göttingen:

Hiermit erkläre ich, dass ich diese Abschlussarbeit selbständig verfasst habe, keine anderen als die angegebenen Quellen und Hilfsmittel benutzt habe und alle Stellen, die wörtlich oder sinngemäß aus veröffentlichten Schriften entnommen wurden, als solche kenntlich gemacht habe.
Darüberhinaus erkläre ich, dass diese Abschlussarbeit nicht, auch nicht auszugsweise, im Rahmen einer nichtbestandenen Prüfung an dieser oder einer anderen Hochschule eingereicht wurde.

Göttingen, den October 6, 2014

(Bartosz F. Guzek)